Stockholm University

Bachelor Thesis

Degree Project in
Marin Geology 30 hp

The origin of Soft Sediment Deformation in the South of Lake Vättern

Ben Knight

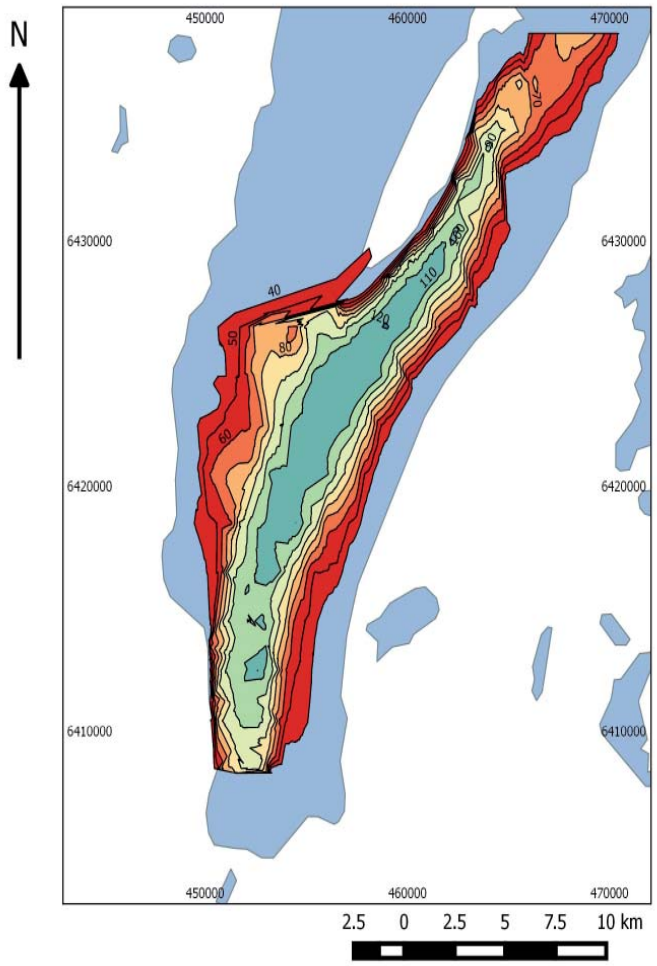

Stockholm 2015

Department of Geological Sciences
Stockholm University
SE-106 91 Stockholm

Abstract

Lake Vättern, Sweden, is situated between two Precambrian terrains in a graben that formed through rifting along the boundary. Geophysical mapping using sub-bottom and reflection methods that were conducted in the region display both glacial erosional features and highly deformed sediment. The sediment structures in the region are interpreted to represent strike-slip sinstral movement that occurred at the end of the younger dryas along a fault that trends along the same strike as the graben structure. Evidence of mass transfer deposits are also seen in the seismic data acquired in the region and are potentially linked to the fault strike-slip fault that is discussed throughout this paper.

Ben Knight
knightBS@cf.ac.uk/bekn5925@su.se

Table of Contents

Introduction

Lake Vättern is located in south Sweden at a mean height of 88.5 m above the RH2000 vertical datum, which was measured between 1940 and 2000 (Jackobsson et al., 2014). It is the second largest lake in Sweden, with an area of 1893 km^2 and a volume of 74 km^3. It is 135 km long, with a maximum width of 31 km. The maximum depth of the lake is 117 m, which was acquired using multibeam sonar, and is located near the southern tip of the lake (Jakobsson et al., 2014). The basin was created by an extensional tectonic regime in the Late Proterozoic (Lindh, 1972; Vidal, 1974) and reactivation of faults in the Phanerozoic, as well as from glacial erosion during the Quaternary (Milnes et al., 1998).

Multibeam and seismic reflection data were collected in 2008 and 2013 in the Southern section of Lake Vättern (figure 1). Sediment cores were taken using a 2.5m long gravity core in 2008, and the upper most 74 m of the sedimentary sequence was cored from a drilling platform in the southern part of the lake in 2012 (Swärd et al., in press).

Hypothesis

The seismic data, along with correlation to cores, should provide evidence to determine the cause of sediment deformation in the Lake Vättern basin. The data should also offer evidence of glacial activity in the region.

Thesis Objectives

The main aim of this thesis is to better understand the history of the area since the last glacial maximum, and can be divided into the following objectives and questions to be answered:

1. Mapping and interpretation of the lake bathymetry
    - What are the main controls on Lake Floor bathymetry?
2. Analysis and interpretation of seismic data
    - What evidence is there of seismic activity in the region?
    - Is there any indication to the presence of a glacier?

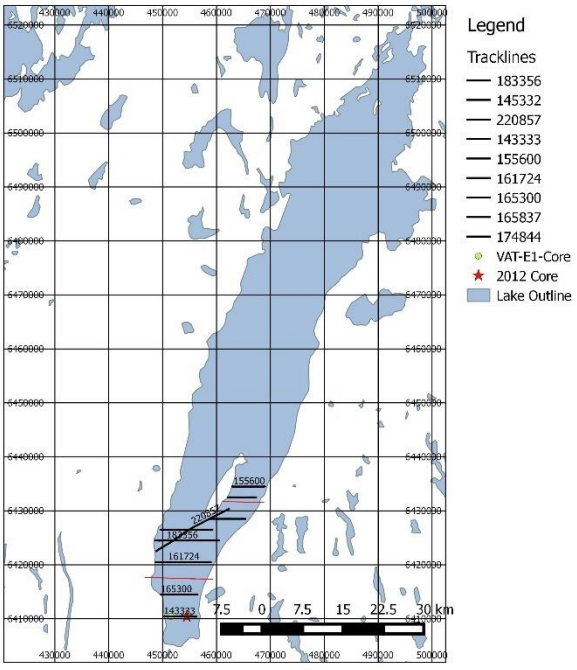

Figure 1: Map of Lake Vättern displaying the positions of the sub-bottom and reflection track lines and cores discussed in this report.

Regional Geology

Lake Vättern is mostly flanked by granites with ages between 1.9 Ga and 1.7 Ga and are part of the Fennoscandian shield, which was subsequently intruded by the Transscandinavian Igenous Belt (TIB) between 1.85 and 1.65 Ga (Söderlund et al., 2005). To the west of the lake, units from the Sveconorwegian orogen, which are part of the TIB (Söderlund et al., 2004), make up the bedrock. Granites and granodiorite are present that have been intruded by igneous mafic rocks, such as gabbro and diabase, and their metamorphic equivalents, with an age around 1.7 Ga (SGU, 2010). To the northwest of these units, older granite is present that has also been intruded by granitoid rock, with an age of 1.8 Ga (SGU, 2010). Further northwest still is another granite and granodiorite that formed 1.8 Ga.

To the east, there is one main granite and granodiorite making up the bedrock of the area, which formed during the Svecokarelian orogen that took place around 1.8 Ga (SGU, 2010). To the northeast of this unit, a Phanerozoic and Neoproterozoic sedimentary bedrock is found, mainly consisting of Sandstone, with some clastic conglomerates and limestone (SGU, 2010). This sedimentary unit is referred to as the 'Visingsö group' and is thought to have formed 0.8-0.7 Ma due to erosion from the Svenconorwegian mountain belt located to the West (Lundqvist et al., 2011). This unit also makes up the bedrock of Lake Vättern, along with small outcrops along the western coast.

Towards the southern tip of the lake, ultrabasic intrusions of gabbro and dioritoid rock are found, along with large areas of rhyolite and dacite extrusions. To the southeast of the lake, doleritic dykes are also found with an age of 1.0 - 0.9 Ga (SGU, 2010). These trend NNE-SSW and are part of the Blekinge-Dalarna dolerites. The intrusions are believed to shallow intrusions based on the observation of sandstone xenoliths and clasts within the dykes that display some primary bedding features (Andréasson and Rhode, 1990). The intrusions are believed to be associated with the later stages of the Svenconorwegian orogen, with emplacement located in the foreland region of the Svenconorwegian orogenic belt (Söderlund et al., 2004) but may also be due to the initial rifting of crust due to their chemical composition (Andréasson and Rhode, 1990).

Lake Vättern is situated near two major tectonic zones, with the Protogine Zone (PZ) to the west and south, and the Sveconorwegian Frontal Deformation Zone (SFDZ) to the North (Figure 2). However, it is unsure if the Lake Vättern is a part of these zones, or if it is an additional tectonic alignment that potentially connects the two. The PZ zone is described by Andréasson and Rodhe (1990) as a major tectonic lineament in southern Sweden, and is traditionally recognised as the eastern boundary of the Sveconorwegian orogen, which occurred 1.1 - 0.9 Ma. South of Lake Vättern, the PZ is a 20-30 km wide system of numerous steep to vertical deformation zones with a predominating dip-slip component. In this area, the PZ defines a metamorphic break between high grade (amphibolite-granulite facies) rocks in the west, against rocks of lower grade (greenschist-amphibolite) in the east. The Westward dipping SFDZ is defined by Wahlgren et al. (1994) as the eastern limit of the Sveconorwegian deformation and metamorphism.

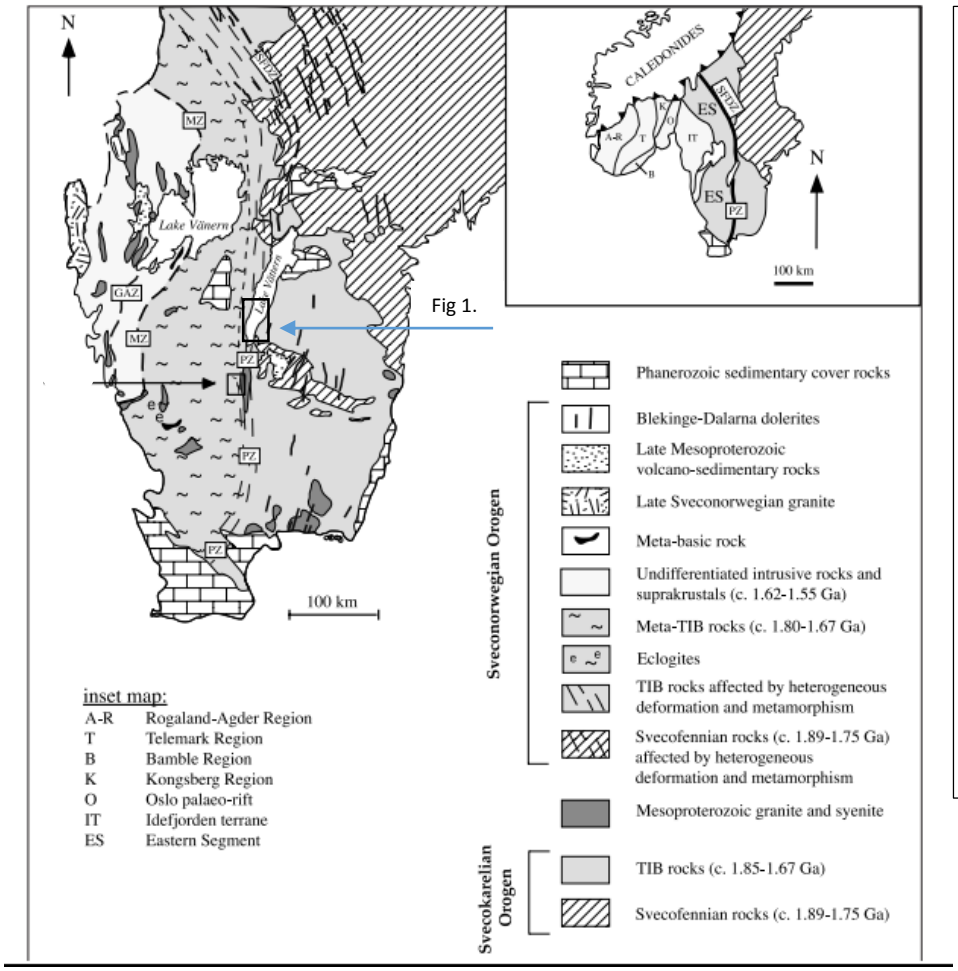

Figure 2: Geological-tectonic map of South Central Sweden. A box displays the location of the research area that is portrayed in figure 1.

Major deformation zones are stippled. GÄZ, Göta Älv Zone; MZ, Mylonite Zone; PZ, Protogine Zone; and SFDZ, Sveconorwegian Frontal Deformation Zone. A thin dashed line marks the northern trace of the PZ.

(Modified from Söderlund et al., 2005)

Formation of the Vättern Basin

The Lake Vättern basin was first described as a graben structure by De Geer (1910). However, questions arising due to the western fault zone made Collini (1951) advocate a half graben structure. Seismic profiling and gravitational mapping of the bedrock beneath the soft sediments by Lind (1972) and Axberg and Wadstein (1980) verified the graben structure that De Geer had first suggested. Two tectonic events are believed to have formed the basin, with the initial faulting occurring at a high angle and dipping to the west. This faulting occurred at the same time as the mid-Vingsö sedimentary unit was formed, with the faulting occurring around 750 Ma (Månsson, 1996). Faulting in the Baltic Sea area that occurred around that time may also be associated with the first phase of rifting in the Vättern rift system (Flodén, 1980).

The second phase of faulting in the basin formed a tilted block structure during the Permian (290 - 240 Ma), forming the lake Vättern graben (Månsson, 1996). This lead to the preservation of around 1000 m of sediments from the Visingsö formation as the downfaulted grabens were protected against profuse erosion. The tilted block graben structure can, for example, also be found in in the northeastern area of southern Sweden (Milnes et al., 1998).

Quaternary Development the Region

Following the last glacial maximum, around 26.5 – 19 ka cal. BP (Clark et al., 2009), the Weichselian ice sheet that covered Northern Eurasia had oscillated between advances and retreats that left traces in the form of ice marginal landforms and deposits that have been used to reconstruct the ice

sheet dynamics, these have been used by Svendsen et al. (2004) to comprehensively reconstruct the late quaternary ice sheet history over Northern Eurasia. The analysis of these geomorphological features, such as moraines, have led to the development of a northward retreat of an east-west extending ice sheet margin that had a convex front over the south Swedish highland and in the Baltic, with both lobes extending southward, calving bays over the deeper parts of the sea (Lundqvist and Wohlfarth, 2001). Seasonal and longer time variations in ice sheet activity are reflected in the seismic profiles as acoustically well stratified units, which are seen in cores as clay varves, comparative to the ones presented by Andrén et al. (2002) from the Baltic Sea. From this, the varve thickness gives an indication of the distance to the ice margin.

According to Björk (2008), the Baltic Ice Lake (BIL) was dammed between the Billingen mesa plateau that is located between Lake Vättern and Vanern, forming a wall between the sea in the west and the BIL in the East. Once the ice had retreated north of Billingen, around 13,000 cal. yr BP, the BIL drained to the west, with the water initially draining under the ice sheet, lowering the BIL by 10 m. However, evidence for this event is believed to have been later destroyed by further ice advances. The younger dryas cooling event then occurred around 12,800 cal. yr BP caused a readvancement of the ice sheet and caused the water level to rise, until Öresund began to function as the main outlet of water. During this period, the main sediment input was glacial. Once the Young dryas period ended (~11,700 cal yr BP), the ice sheet once again retreated north. This unblocked the passage between Billingen and the sea to the west. As the Oresund threshold was around 25m above sea level at this point, the opening of the Billingen passage caused a sudden large drop in the BIL level of around 25m in around 1-2 years and released an estimated 7,800 km^3 of fresh water into the North Atlantic Ocean (Jakobsson et al., 2007). This is documented as large deposits of boulders and pebbles that are have been deposited during this event and are located 5 - 7 km west of Billingen and marked the beginning of the Yoldia sea stage.

Reactivation of faults occurred at the end of the Younger Dryas period occurred, with a fault movement that generated a potential maximum magnitude (M_w) of 7.5 earthquake, with a maximum displacement of 13 m and rupture length of 125 km, which was determined by empirical relationships. However, a sense of movement of the fault has yet to be determined (Jakobsson et al., 2014). This fault movement may have been due to the unloading of the glacial ice sheet or the sudden drainage of around 7800 km^3 of water from the Baltic Ice Lake, but most likely a combination of the two (Jakobsson et al., 2014).

Seismic Theory

Two Way Travel Time

During all surveys, except side-scan sonar, a two-way travel time (TWTT) is recorded by the device, which is then converted to a depth using the formula:

$$d = \frac{t}{2} \cdot v \quad (1)$$

Where *d* = Distance, *t* = Two Way Travel Time (TWTT) and *v* = Velocity.

$$v = f \cdot \lambda \quad (2)$$

Where *f* = frequency and λ = wavelength

This is then used to convert time profiles into depth profiles. However, as the sound velocity through different mediums changes, the time profiles do not reflect the true thickness of the units. This is resolved by applying the different speeds for different units and usually results in different sizes of bodies in between the time and depth profiles. When focusing on the surface in multibeam or chirp sonar, the harmonic mean of the speed of sound is calculated to determine the surface features, which is explained more in the sound velocity profiles, below. The relationship between frequency and wavelength is important, due to higher frequencies resulting in shorter wavelengths, which gives a higher resolution but less penetration, whereas lower frequencies result in longer wavelengths and thus further penetration.

Vertical Resolution

The vertical resolution of any seismic survey is determined by the Rayleigh criterion. This is the thickness of reflective criterion, or the minimum vertical distance between two reflective boundaries that can be resolved as separate entities on a seismic profile due to wave interference. This differs between theory and in seismic surveys, where in theory the criterion is about λ/4, whilst in seismic surveys the criterion is closer to λ/2 (Trabant, 1984).

Horizontal Resolution

For the horizontal resolution, only reflections from within the first Fresnel zone can be used as energy is dissipated from the air gun in all directions and outside this zone, destructive interference occurs. This can be determined by the following formula:

$$R_f = \sqrt{\frac{h\lambda}{2} + \frac{\lambda^2}{16}} \; where \; \frac{h\lambda}{2} \gg \frac{\lambda^2}{16} \quad (3)$$

Where R_f is the first Fresnel radius, *h* is the height of the water column, and λ is the wavelegth

This causes some distortion in the data as it makes narrow troughs and high peaks hard to map accurately as they appear as a point source on the seismic data, forming a parabola in the seismic data.

2.4 Reflection Criterion

In the seismic profiles there are clear boundaries that are visible. These boundaries are created due to a reflection being caused at a boundary between two different units that have a different acoustic

impedance, which is a product of the units density (ρ) and p-wave velocity (v) (Kearey et al., 2002). This gives rise to the reflective coefficient, which is a measure of how much of the seismic energy is reflected at the boundary. To determine the reflective coefficient, formula (4) is used:

$$\Gamma = \frac{Z_1 - Z_0}{Z_1 + Z_0} \quad (4)$$

Where Γ = reflective coefficient, Z = acoustic impedance, where Z_1 is the unit/layer below Z_0.

Two important parameters of the seismic P-waves are their velocity and frequency. The P-wave velocity is variable through the stratigraphic successions, being directly controlled by of the lithological composition, porosity, density, texture, pore-water, compaction, elastic modulus and also fluid content. In general, velocity tends to increase with depth as rocks become more compacted (Brown, 2004; Kearey et al., 2002). In contrast, acoustic frequency consists in the number of wave cycles passing by one point per second, and this tends to decrease with depth as the higher frequencies preferentially attenuate while travelling through the rock (Brown, 2004). The larger the reflective coefficient, the more noticeable the boundary appears on seismic profiles. If a negative reflective coefficient is present, then a phase shift of 180^o occurs, causing the opposite polarity when compared to the original signal. This occurs when, for example, the sound pulse interacts with a gas that has occupied the sediment pore space.

Data Acquisition

Multibeam

Multibeam data was collected in 2008 with a Kongsberg EM3002D, 300 kHz 1.5° × 1.5° multibeam that was bow mounted on the 11-m long vessel *Cappella*. Locations were determined with a Hemisphere A100 GPS utilising the geostationary satellite-augmentation system corrections SBAS. These augmentations account for satellite position errors, satellite clock/time errors and errors induced by the signal travelling through the atmosphere, which increases the accuracy of positioning to within 1m (Navipedia, 2015). Motion sensor data was acquired by a Seatex MRU5, which corrected the data for yaw, pitch, roll and heave.

Mapping continued in 2013 with a Kongsberg EM2040, 200–400 kHz 1° × 1° MB bow mounted on the 6.4-m-long survey boat *RV Skidbladner*. Positions were resolved using a Hemisphere R320 GPS, corrected by the Swedish SWEPOS system, a network of permanent GPS reference stations, to obtain full real-time kinematic (RTK) accuracy. This system exploits the carrier phase of a signal to increase the horizontal accuracy of position to within 2-6 cm. RTK also allows the use of GPS height and vertical referencing of the depth data directly to the WGS 84 ellipsoid. In turn, this permits a transformation from WGS 84 to Mean Sea Level (MSL) using a geoid separation model. During the Vättern survey in 2013, the Swedish geoid model SWEN08_RH2000 was used for this purpose (Martin Jakobsson, personal communication). The final reported depths from the multibeam survey are referenced to a mean lake level of 88.5 m above the vertical datum RH2000, equivalent to MSL (Martin Jakobsson, personal communication).

Multibeam data is useful for providing highly detailed and georeferenced information of the lake floor. The main difference between multibeam and other seismic data acquisition comes from the source of the seismic wavelet, with an array transducers used instead of just one in the chirp and/or air gun data acquisition. A fan-like front is formed from the multiple sources, which cover a wide portion of the lake-floor (Figure 3b). The depth at a reflection point (y, z) is calculated using the TWTT, as stated in formula (1), along with the incident angle θ and the sound velocity profile, which is determined using a sound velocity probe (Randall, 2008; Lurton, 2010). The locations are determined by the following formulas:

$$y = D\ sin\theta = \frac{vt}{2} sin\theta$$

Where y = distance from the ecosounder, θ = beam angle from the vertical, v = sound velocity in water, D = distance and t = two-way travel time

$$z = D\ cos\theta = \frac{vt}{2} cos\theta$$

Where z = vertical distance from transducer to lake floor.

The main benefit of using multibeam bathymetry compared when compared to other seismic data acquisition is the ability to more accurately determine the geographic location of the data points that are generated as georeferenced depths and reflective data are collected simultaneously (Lurton, 2010).

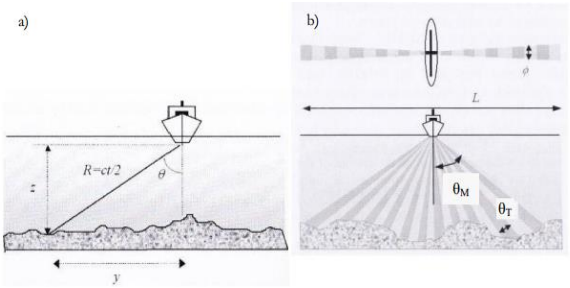

Figure 3: a) visual representation of the position of z and y. b) Top: birds eye view, where L is the swath with and ϕ is the along tack angle. Bottom: Profile view, where Θ_M is the maximum beam tilt angle, Θ_T is the across-track beam angle. (Lurton, 2010)

Sub-Bottom Profiling

Subbottom profiling was carried out in 2008 and 2013. In 2008, an EdgeTech SB216 tow fish that has a range of 2-16 kHz, whilst a 20 millisecond long chirp pulse that oscillated between 2–12 kHz was used, whilst a Kongsberg EA600 15 kHz echo sounder was used in 2013 profiling. GPS positions were acquired using a Hemisphere A100 augmented with SBAS, whilst and motion sensor data was acquired by the Seatex MRU5.

Sub-bottom profiling utilises chirp-sonar that is based on the principle of emitting a wavelet, a sound pulse that initially increases in frequency, before peaking and then returning to its original frequency in a set time. This signal is emitted by a piezoelectric transducer, where a sound pulse is created by an electric potential causing a mechanical stress to the material. This change in frequency, also known as a 'signature pulse' allows the reflected wave from any boundaries to be easily identified in any background noise due to matched filtering (Schock et al. 1989), also known as 'pattern matching' techniques (Christ and Wernli, 2014), which matches the unique signature of the outgoing pulse with the incoming reflections.

During the 2008 survey, a 2-16kHz EdgeTech SB-216S Sub-Bottom profiler was used, which utilises a low Q- filter that allows a wide pass band, as well as two multi element line array hydrophones, which reduce acoustic scattering at the sides, and a linear power amplifier, which generates harmonic free transmissions (Sonographics, 2014), allowing for a clearer image of the sub-surface sediment to be created from the data recorded. A 2-12 kHz frequency range was used as it gives us ample penetration of the sediments (up to 60 m in clay) whereas a higher frequency would not penetrate as far into the sediment. In comparison, navigation echo sounders, used only for depth perception, usually operate at a frequency between 30-200 kHz.

Reflection Profiling

Seismic reflection profiling was carried out in 2013 with a ~0.3 dm^3 (20 in^3) Bolt PAR airgun and an 18 m long hydrophone streamer on the 10-m long vessel *Hamnen*.

Air guns utilise the decompression of air released from the air gun chamber, which causes an oscillating bubble to form. Due to the difference in pressure, the bubble initially expands until the external water, or hydrostatic, pressure acting on the bubble is greater than the internal air pressure, causing it to start contracting. This results in a continued oscillation as the bubble does not reach equilibrium, with a typical period in the range of tens to hundreds of milliseconds. The oscillation of the bubble, until it breaks the surface due to its buoyancy, causes multiple seismic sources which is far from the ideal, single peak seismic source (Parkes and Hatton, 1986). To combat

the bubble bounce, the airgun used was equipped with a 'wave shaping kit', which is a 2nd chamber that injects air into the pulse to prevent a bubble pulse forming

As the energy from the air gun dissipates in all directions, a reflection occurs at the water-air boundary, creating a 'surface ghost'. This surface ghost affectively doubles the amplitude, but has an opposite polarity to the original source. This ghost also causes the removal of lower amplitudes (known as the ghost notch effect), so the source must be located near to the surface of the water (OGP report, 2011).

Hydrophones record the pressure change in the water column that is caused by the presence of p-waves caused by the air gun. The hydrophones utilise the piezoelectric effect, which is where an electrical signal is generated when a material undergoes stress. This electric signal is then transmitted via cables on-board, where it first goes through amplification and then is processed by computers to produce a seismic reflection image. Amplification is required due to energy lost in the original signal through friction between the sound wave and its surroundings, with the main energy lost due to geometric spreading as the wave propagates from the source in all directions (OGP Report, 2011).

Sound velocity profiles

Sound velocity profiles were conducted for the correction of the multibeam data, as well as using the data to convert two-way travel time to depth. The data was acquired using an Applied Microsystems (now AMLOceanographic) sound velocity probe to record the conductivity, temperature, depth (CTD) and sound velocity that could be used to determine the velocity profile during each multibeam survey. During the 2008 survey, an issue caused the probe to stop working, so a thermometer was used instead to collect temperature readings, although this caused severe refraction problems due to large temperature changes within the lake. Problems also occurred with the device mounted near the transducer, reducing the usability of the data. During the 2013 surveying, multiple readings were taken each day using the CTD probe, as well as from the device mounted near the transducer.

Coring

Gravity cores allow a direct sample to be taken from the lake floor. A winch is used to lower the core down to the lake floor under its own weight, which is guided by fins to keep it straight, and then inserts into the sediment. Extra weights are added to the core to allow this to occur. Once the core has been fully collected, the core is extracted to the surface using the winch, with the core remaining in place via a core catcher, or Madonna bra. The benefits of using a gravity core are that it is simple, cheap to run and maintain, robust as well as easy to deploy, however it is heavy and awkward to manoeuvre, requiring a large enough vessel and winch to be used (Steele et al., 2001).

In October 2012, sediment coring and drilling were conducted from a floating barge equipped with a drill rig by Asera Mining Ltd.. The rig drilled down into the bedrock of southern Lake Vättern to a distance of 74 m below lake level for mine prospecting purposes. The sediment coring system consisted of tools added to an HQ wireline drilling system, including HQ-3 plastic liners (inner ϕ 63 mm) for collection of unconsolidated sediment (Jakobsson et al., 2014).

Data Processing

Seismic Data

Sub-bottom and reflection data was processed and analysed using the OpendTect software suite. Initially, the native SEGY files were troublesome to import, with the coordinates firstly requiring a conversion using the Geological Survey of Canada (courtesy, Bob Courtney) SEGY Navigational converter. This converted the geodetic coordinates to UTM zone-33 coordinates, using an internal coordinate divisor of 3,600,000 as well as a coordinate multiplier of 100. Once the coordinates had been converted, a 'tracr' number had to be inserted into the data, which represents the trace sequence number within reel of the entire data set (Forel, Benz and Pennington, 2005). This was completed on both the sub-bottom and reflection data, on each line individually, using the manipulate feature that is present on the 'import seismics' window, with an 'indexnr' formula used to modify the trace sequence. Once the 'tracr' number had been modified, the seismic lines could then be imported and then viewed in the 2D window (figure 4), as well as the scene window (figure 5).

Figure 4: 2D viewer displaying seismic reflection data.

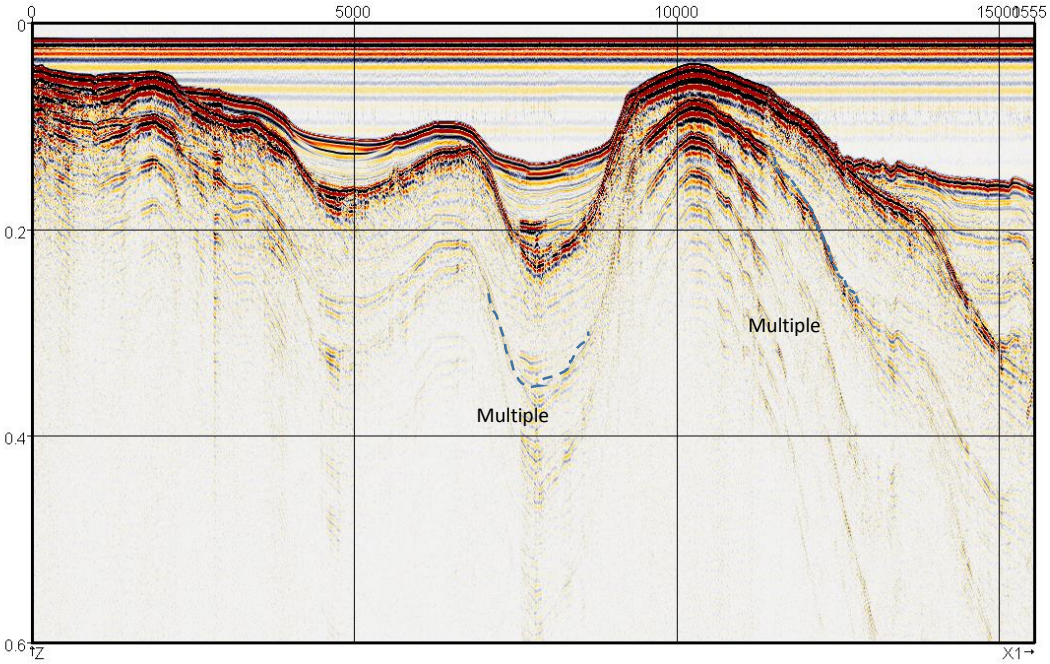

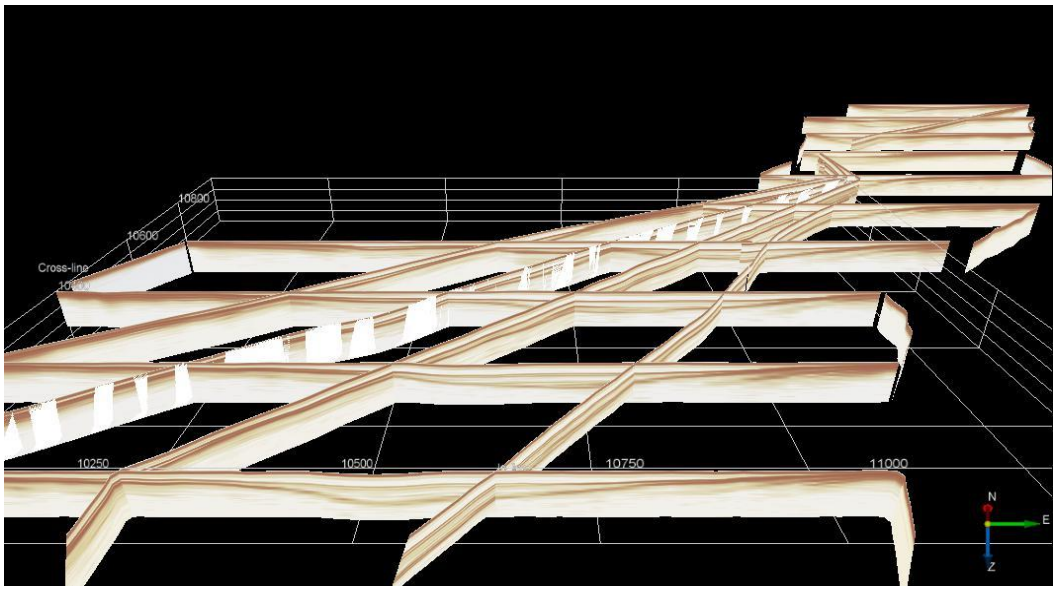

Figure 5: Scene view, displaying all of the 2D seismic reflection data in a 3D grid that can be maneuvered to view the data from different angles.

After all the data had been imported, horizons were traced using the 2D horizon tool that allows tracking from the 2D viewer window. This was then used to create a bathymetric map of the mapping area, as well as a bedrock map.

Sound Velocity Profiles

Data from the velocity probes returned a velocity and depth that was space separated. This data was imported into excel to create the velocity profiles by plotting velocity against depth (figure 6). The harmonic mean was also calculated from the data, which is defined as the reciprocal of the arithmetic mean of the reciprocals of a set of specified numbers (Collins English Dictionary, 2003). Due to limitations of the software, the harmonic mean calculated for all 7 data sets was used to convert two-way travel time to depth, which was then used for the bathymetric map (table 1).

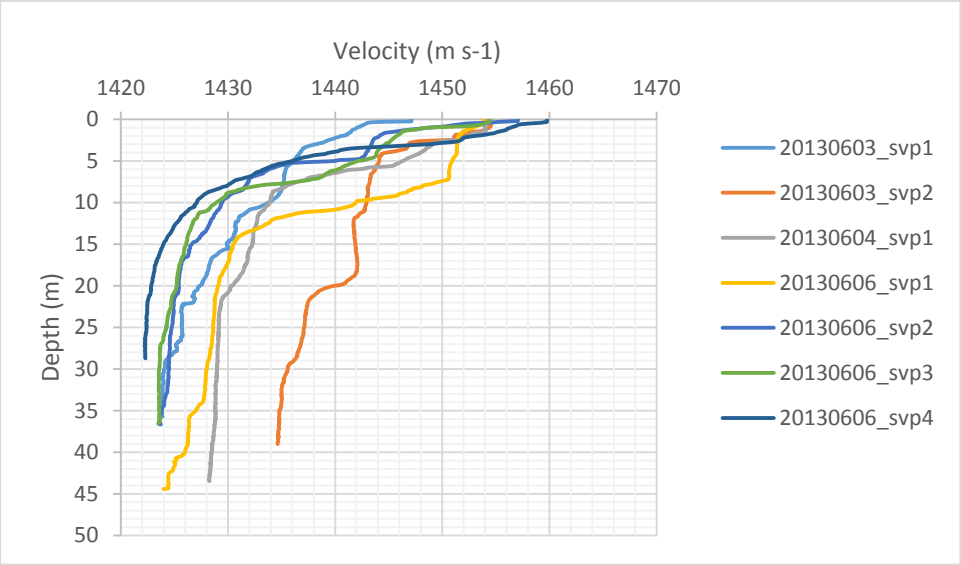

Figure 6: Sound velocity profiles from Lake Vättern, taken on 3 consecutive days in June, 2013

Profile Name	Harmonic Mean
20130603_spv1	1429.777553
20130603_spv2	1440.933699
20130604_spv1	1432.893877
20130606_spv1	1434.481351
20130606_spv2	1429.859592
20130606_spv3	1429.995745
20130606_spv4	1428.862031
all profiles	1432.389713
Standard Deviation	3.9466

Table 1: Harmonic mean values calculated for each probe, as well as the harmonic mean of all 7.

Observations

Bathymetric Map

The bathymetric map in figure 8 was created using the 3D horizon generator from a 2D horizon in the OpendTect software suite, using the irregular triangulation network (ITN) method. This data set was then exported to an ASCII format file, and then imported into the QGIS software suite using the 'add delimited text layer' feature. Once imported, the file appeared as a point data set due to each coordinate being associated with a depth. This was then created into a contour map using the 'contour' plugin that allows contour lines and filled contours to be generated from point data. Following this, the contours were then smoothed using the geometry tool 'simplify geometries', resulting in figure 8. Errors in the depth arise from the distance the device was towed below the lake surface, as well as from the use of a harmonic mean from all sound velocity profiles taken in the area.

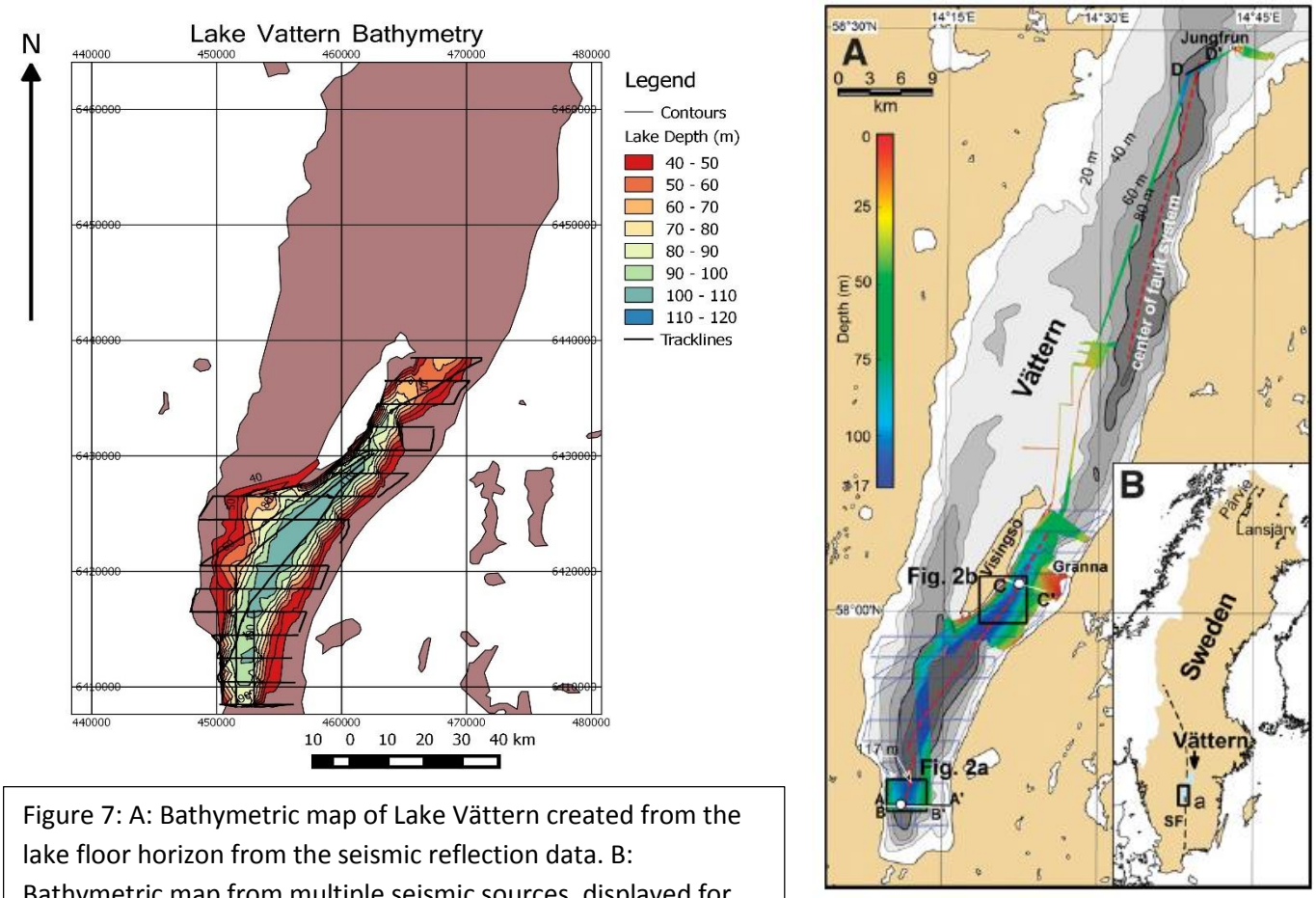

Figure 7: A: Bathymetric map of Lake Vättern created from the lake floor horizon from the seismic reflection data. B: Bathymetric map from multiple seismic sources, displayed for comparison (Jakobsson et al., 2014).

From figure 7A, a deep zone can be seen that trends NE of the map, with a depth that does not become shallower than 100m for a substantial area in the centre south of Visingsö. Due to the nature of the data acquisition and processing, where smoothing took place and the sampling between seismic lines, which does not provide a true representation of the bathymetry of the lake. However, the existence of this deep channel is important as it is present due to the lakes tectonic history and subsequent evolution, including erosion by the Quaternary ice sheets. When comparing

to the bathymetric image produced by Jakobsson et al. (2014) in figure 7B, the two correlate well, with the contour lines located in similar positions.

Seismic Reflection and Sub-bottom

Seismic Stratigraphy

The gravity cores taken in 2008 and the sediment core drilled in 2013, along with the subsequent analysis, allows a better understanding of what boundaries are causing reflections, as well as the position of the bedrock in the seismic profiles. Density and P-wave velocity measurements were made on the 74m long core, this allowed an acoustic impedance to be determined, which made identifying clear changes in the sediment easier. From the data acquired by Swärd et al. (in press), 3 units were identified, along with multiple sub-units in each, which is summarized in table two.

Unit	Top (mblf)	Base (mblf)	Interpreted Unit	Impedance (kg m^{-2} s^{-1})	Reflective Criterion	Harmonic Mean (m s^{-1})
Unit 1:	**0**	**15**	**Gyttja Clay**	**1939.65**		**1482**
Subunit 1A	0	10		1879.01		1482
Subunit 1B	10	15		2024.56		1481
					0.095	
Unit 2:	**15**	**25**	**Post Glacial Clay**	**2347.41**		**1481**
Subunit 2A	15	22		2301.43		
Subunit 2B	22	25		2421.11		
					0.090	
Unit 3:	**25**	**75**	**Glacial Clay**	**2817**		**1523**
Subunit 3A-3B	25	55		2684		1502
Subunit 3C	55	70		3165		1568

Table 2: Summary of the sedimentary units found in the seismic profiles from analysis.

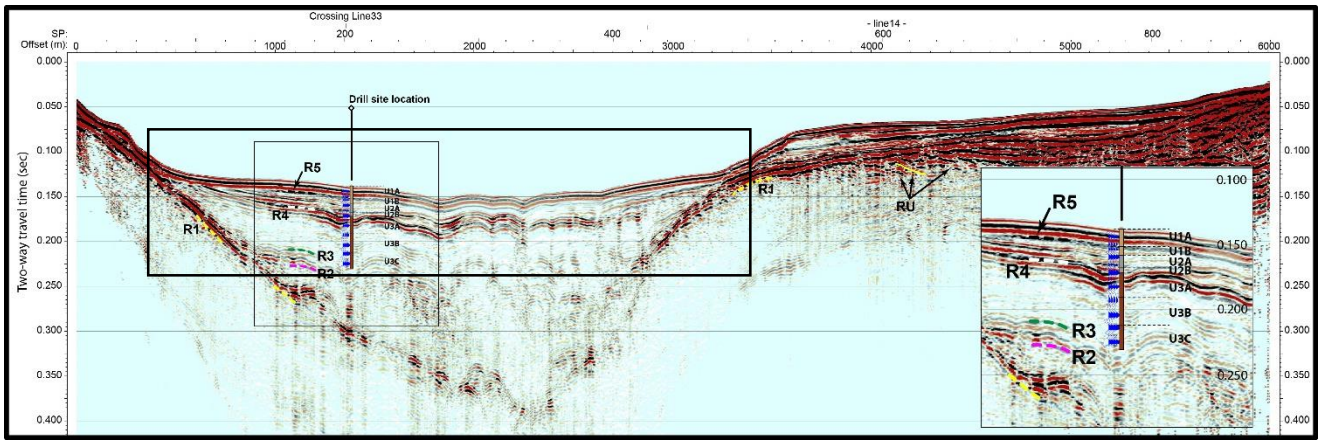

A

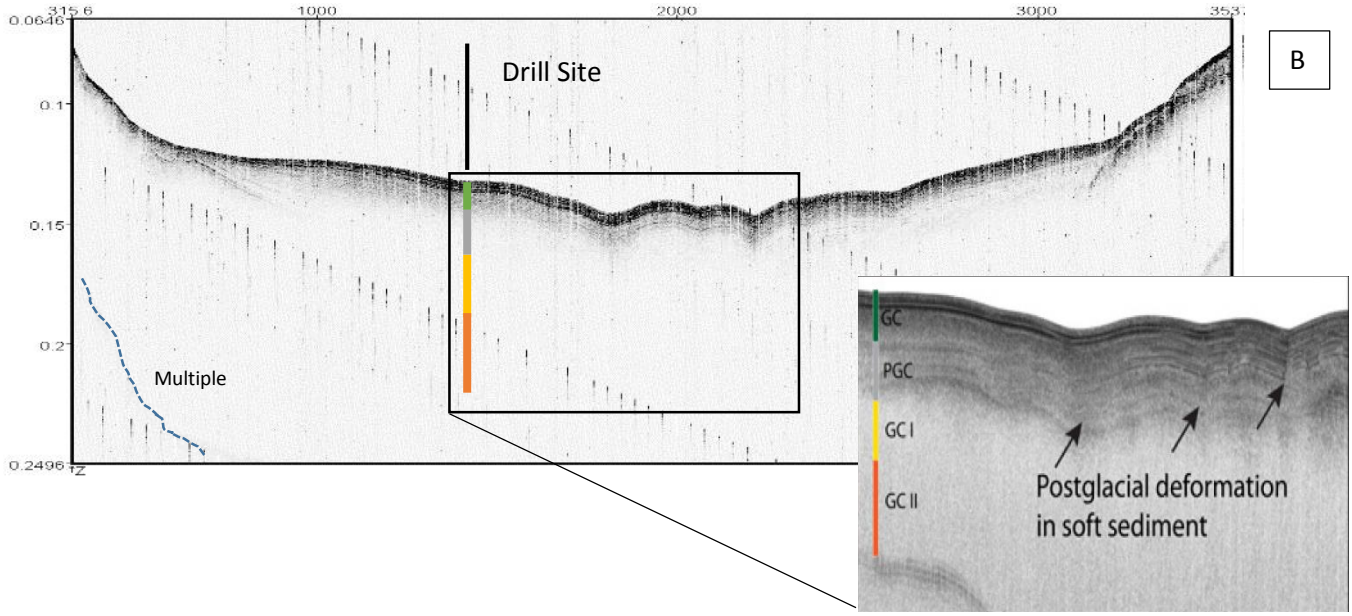

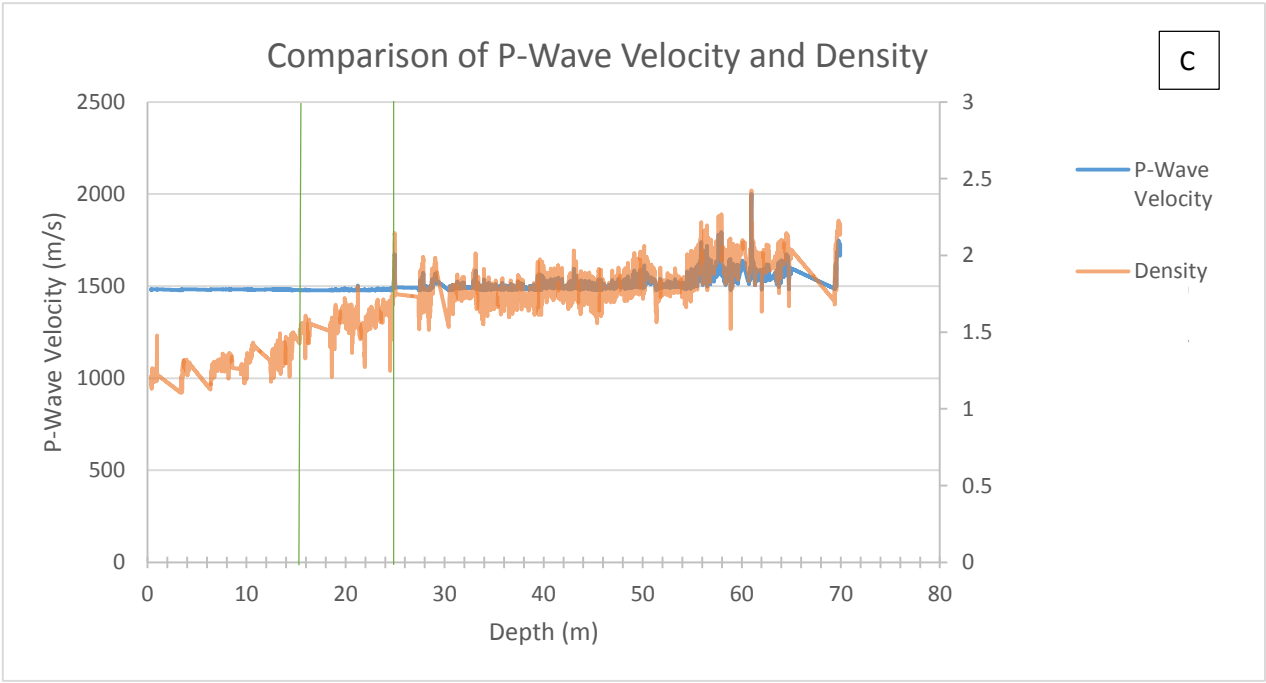

Figure 8: A: Seismic reflection profile of Line 143333 across the graben in the southern part of Lake Vättern, with black box signifying the position of B (Swärd et al. (in press). B: Subbottom profile B-B' (TWT—two-way travel time). Major stratigraphic boundaries are inserted (U3 —glacial clay unit II (GCII); U3A/B—glacial clay unit I (GCI); U2 —postglacial clay (PG); U1 —gyttja clay (GC)) (Jakobsson et al., 2014). C: Graph displaying the P-wave velocity and density to determine the main causes of

From the reflection data in figure 8A, unit 1 is characterised by a high amplitude, sub-horizontally layered reflectors and is the youngest sediment layer in the sedimentary stratigraphy. From figure 8, the main cause of this large reflection between units 1 and 2 is due to a change in the P-wave velocity of the unit. Unit 2 is characterised by a low-amplitude unit that appears to have only a small

reflection present towards the base, which occurs due to the change in stratigraphy from unit 2A to 2B. Figure 8C displays that the reflection between unit 2 and 3 is caused by an initial decrease and then a sudden large increase in density between the two units. Unit 3 is characterised by a high amplitude reflector at the boundary between 2 and 3, along with multiple strong reflective boundaries throughout the unit. The blue seismic traces displayed next to the core in figure 8A represent a synthetic seismogram that was created using the density and velocity data from the drill core. This synthetic records was generated by Swärd et al (in press) in order to correlate the seismic stratigraphy with the sediment core stratigraphy. The boundaries are slightly harder to determine in the subbottom profile (figure 8B), although they can be deduced from the insert image. Unit 1 is characterised by a dark grey layer that has some horizontal reflectors. Unit 2 appears lighter than unit 1, with horizontal reflectors present throughout the unit. Unit 3 is lighter than the previous two and displays no horizontal reflectors. These units are shown on all interpreted profiles, with unit 1 olive green, unit 2 is blue, unit 3 is purple and the bedrock reflector is red.

Seismic Profiles

Multiple seismic profiles were acquired across the lake, with the position of these depicted in figure 1 and 7A. As well as using the seismic reflection profiles to create the bathymetric maps, they were also used to analyze deformation of the sediment and bedrock to determine age constraints of tectonic events using the correlation between the seismic profiles and cores as seen in figure 8A and B.

Sediment Deformation

Throughout the study area, many different types of deformation are visible in the sediment that has been deposited. According to Steno's Law of Superstition 'in any sequence of sedimentary rocks which has not been disturbed, the oldest strata lie at the bottom and the youngest at the top'. This can be applied to the sediments present below the lake floor but above the bedrock, with any deformation that has been caused and is visible in the seismic profile can be linked to either tectonic activity in the area, glacial activity, mass wasting or bottom currents.

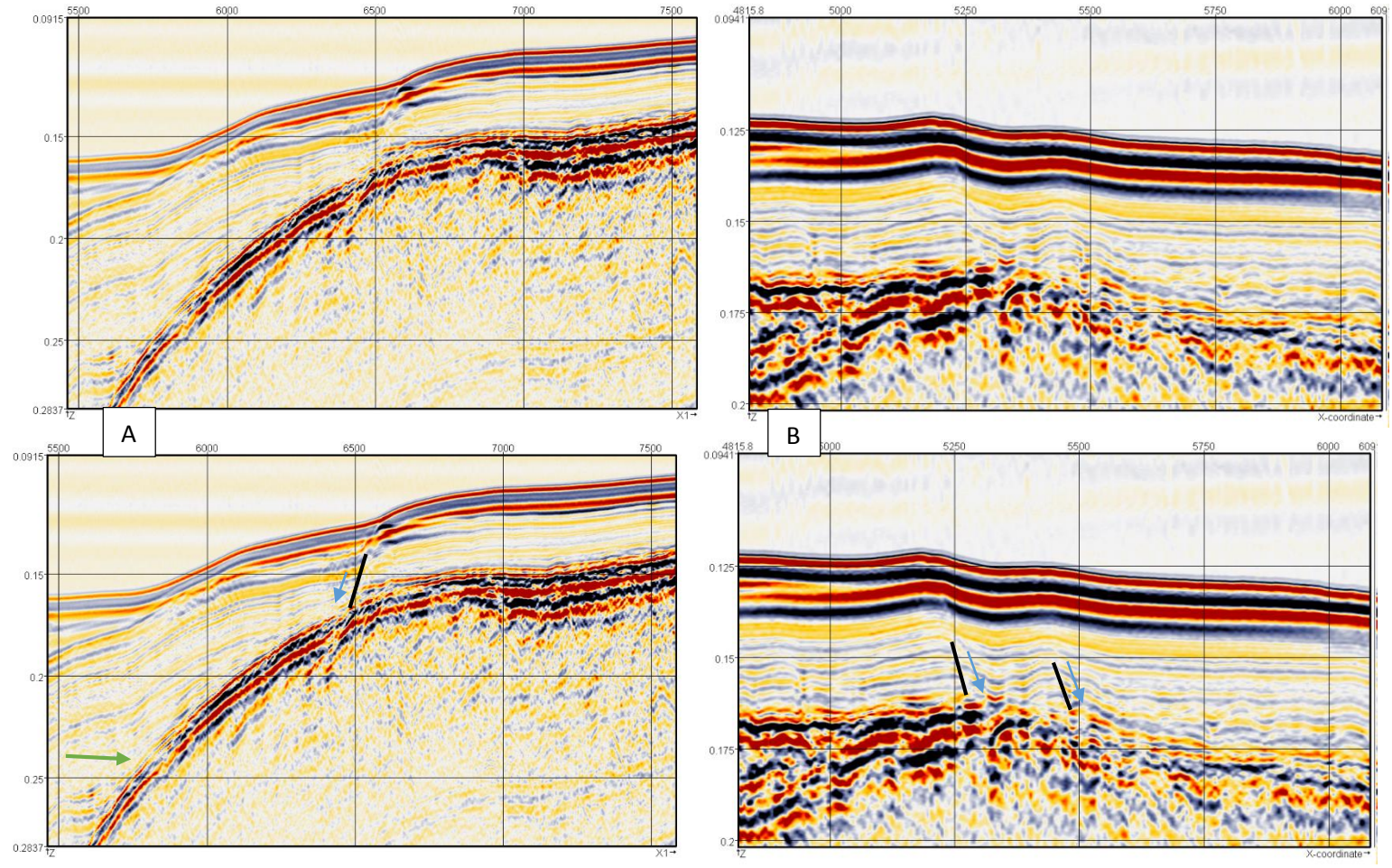

Figure 9: A: Seismic profile of Line 161724. B: Seismic profile from line 183356. Both show sediment deformation that concaves upwards.

Figure 9 displays two different seismic profiles that appear to show the movement of sediments in in a downslope direction. In Figure 9A, the surrounding sediment appears mostly horizontal to sub-horizontal, with only some on-lap present near to the lake floor (green arrow). In figure 9B, two elevations in near proximity can be seen from the seismic profile, with a slight depression between the two. The reflections from both appear discontinuous, with breaks appearing in reflections. Either side of these elevated areas, the rest of the sediment appears mostly horizontal to sub-horizontal, with the steepest reflectors present between the two elevated areas. In both of these, the faults appear in the lowermost sediment, interpreted to be glacial clay, but have affected the entire sediment above, making it a recent feature.

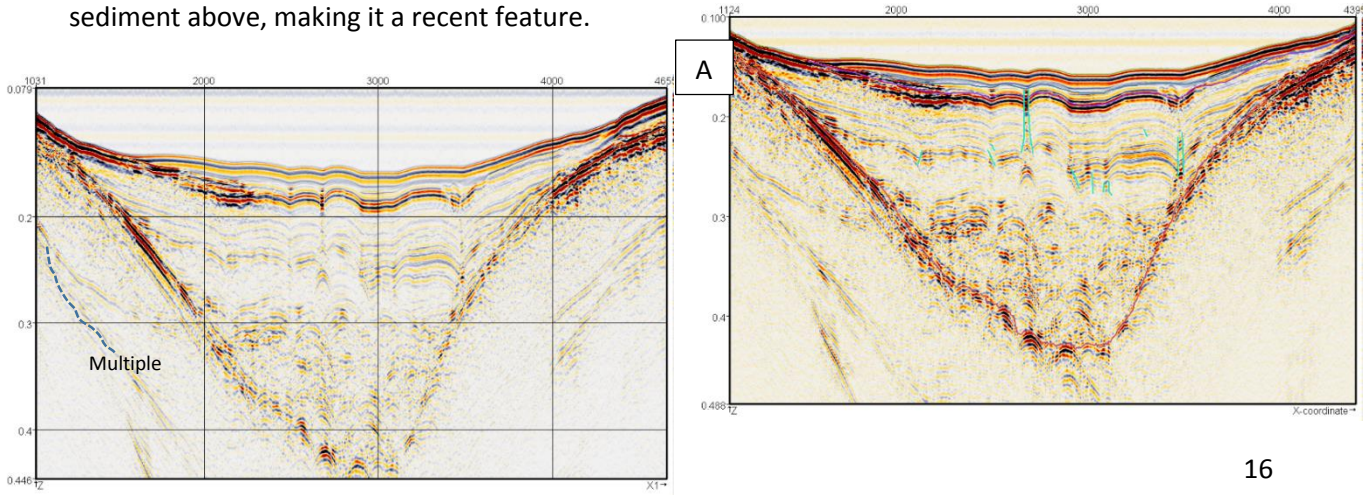

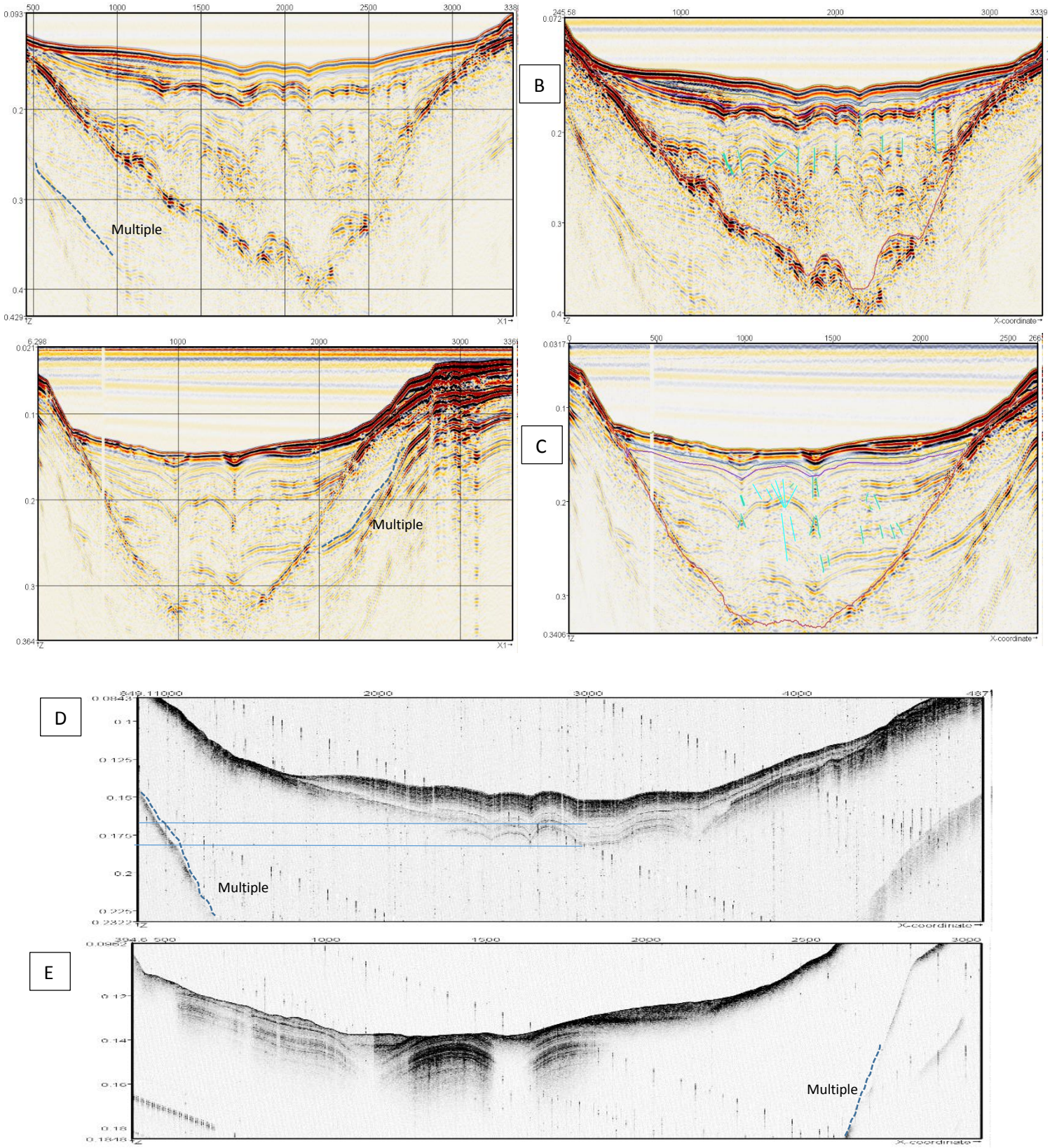

Figure 10: A: seismic profile of Line 165300. B: Seismic profile of Line 143333. C: Seismic profile of Line 174844. All display large sediment deformation in the centre of the graben. D: Sub-bottom profile of line A. E: Sub-bottom profile of line C.

Figure 10 A and B show similar deformations as both are taken perpendicular to the strike of the graben. From the reflectors present in both, sediment can be seen to concave upwards in both profiles. This appears to affect the entire sediment column above the bedrock, which is interpreted as the last strong reflector near the bottom of the profile (red line). The main zone of deformation is concentrated in the center, with multiple synforms and antiforms present, which are displayed as alternating areas of elevation and depressions across the top strong reflector, and then continue throughout the sediment column. As the two-way time increases, these synforms appear in a 'bow-tie' shape and the antiforms appear as a hyperbola due to the profiles being unmigrated. Either side of these elevations and depressions, the slope gradient maintains fairly constant, with only a slight undulating surface, with the reflectors appearing horizontal to sub-horizontal. Figure 10A and B also display toplap of glacial clay to gyttja clay. Figure 10C is similar to those portrayed in figure 10A and B, however the difference between them is apparent in the uppermost sediment layer. Figure 10A and B has the deformed layer exposed at the lake surface, however in figure 10C the synform structures appear to have filled in and draping has occurred, which is most likely with gyttja clay sediment. When analyzing the sub-bottom profiles in figure 10 D and E, this confirms the draping of gyttja clay in profiles 174844 and the apparent deformation of gyttja clay in profiles 165300 and 143333. The symmetrical folding in the sediment is substantial as they have an amplitude of around 0.01 seconds, which is the equivalent of around 7.6 m from the inflection point.

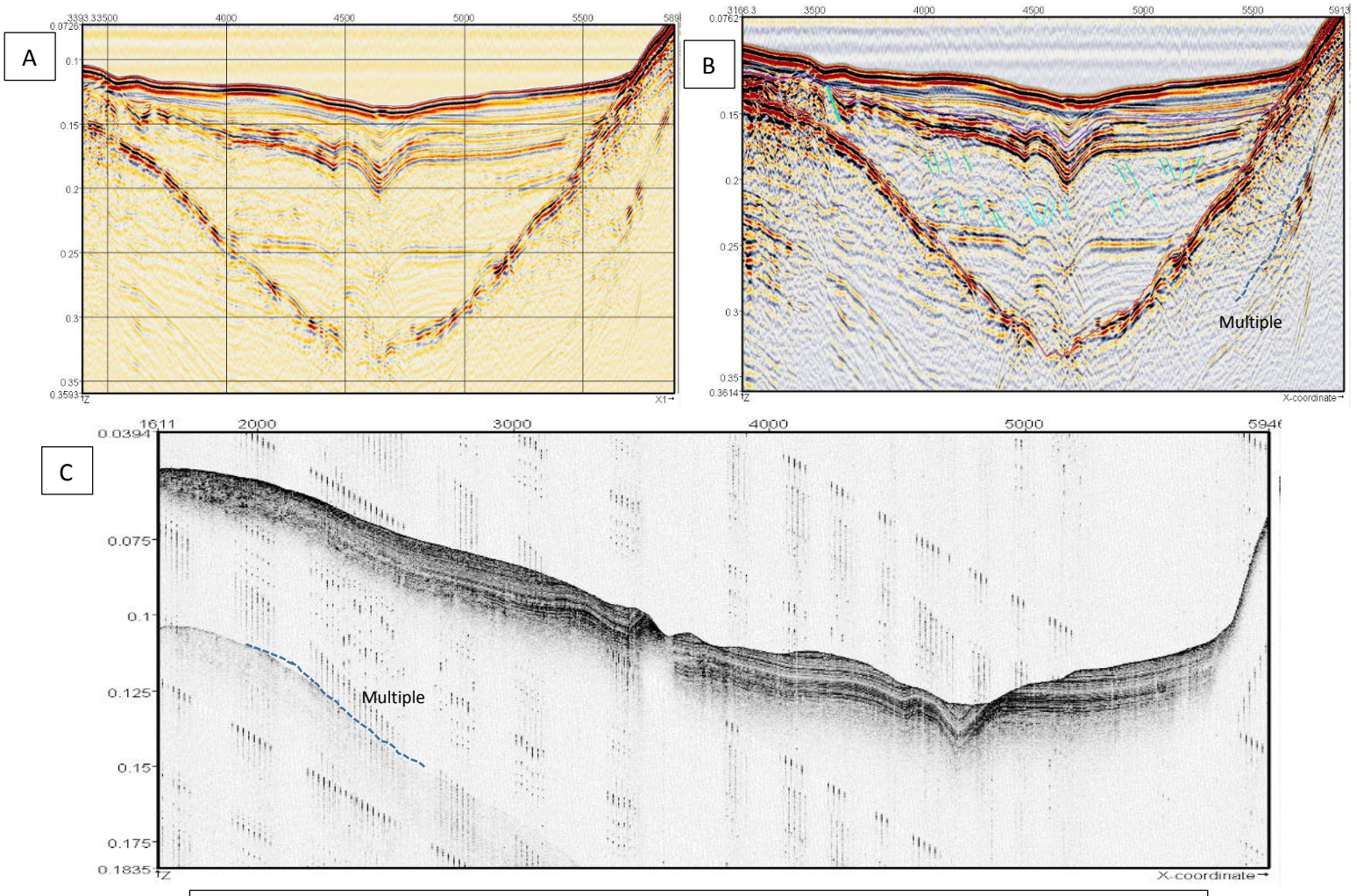

Figure 11: Seismic profile of line 155600 showing deformation of deposited sediments. A: Original reflection data. B: Interpreted reflection data. C: Sub-bottom profile.

Figure 11 displays a profile also taken perpendicular to the strike of the Vättern graben. In the seismic profiles, the uppermost sediment unit (gyttja clay) appears to have undergone little or no deformation and is draped on top of the post glacial clay. Underneath these, the sediment appears to have undergone a large deformation that effects all sediment up to post-glacial clay. However, when analyzing figure 11C, there is little presence of gyttja clay. Instead, the area has undergone profuse erosion, with the lake floor sediment mainly consisting of glacial clay. A large depression can be seen at around trace number 4625, where the glacial clay has been deformed and eroded, with a small deposit of gyttja clay in the center. The sediment across the rest of the profile seems to be in its original near-horizontal depositional position with little or no disturbance when compared to these two large areas of deformation. When compared to figure 10, figure 11 portrays a much larger and obvious depression due to the strength of the reflectors, which originate from the glacial clay unit.

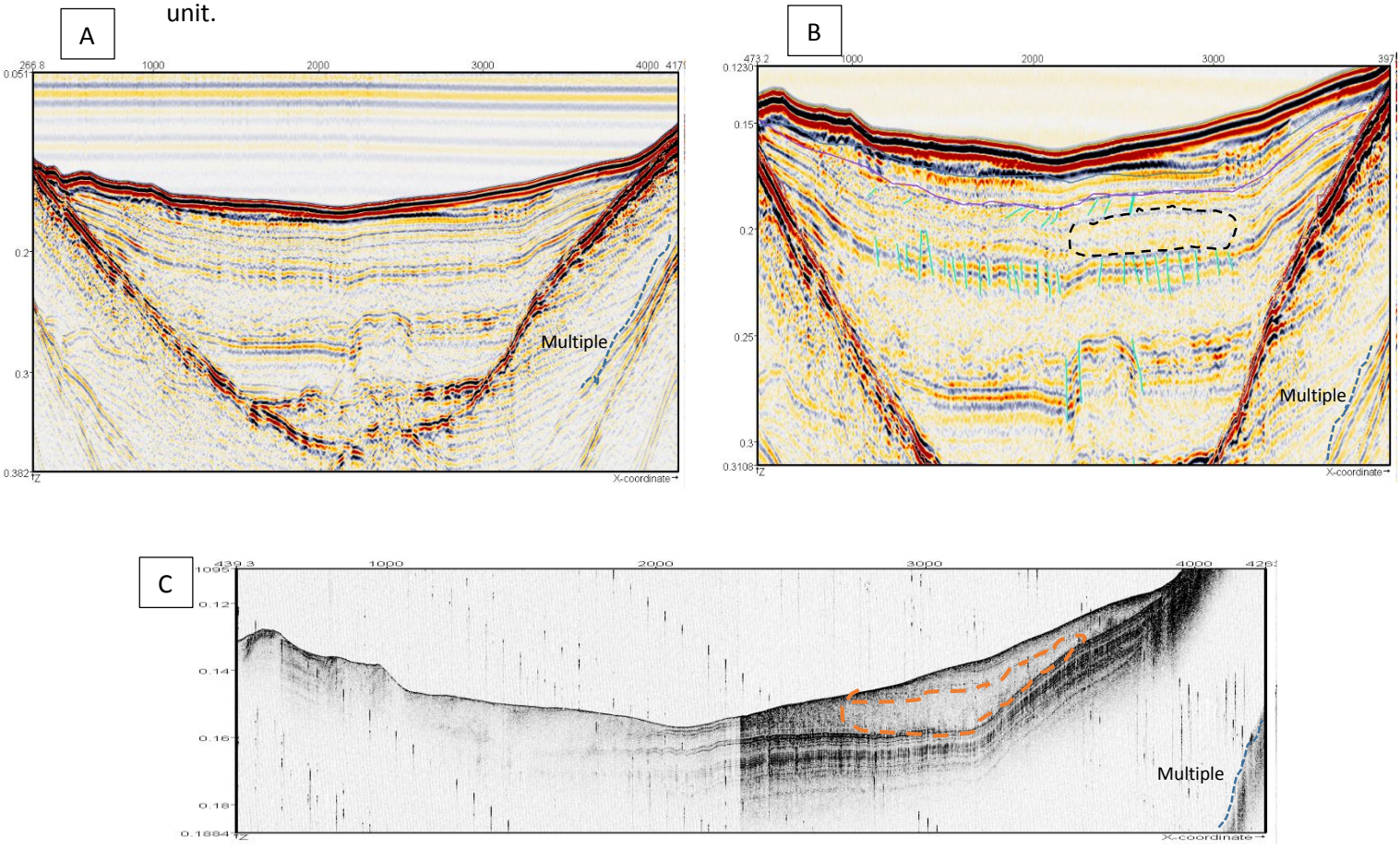

Figure 12: A: Seismic reflection profile of line 145332. B: Interpreted line of A showing a potential paleo-landslide (black dashed line). C: Sub-bottom profile of line A.

Figure 12A and B displays the seismic reflection profile of line 145332. The area that is encircled by a dashed line represents a low-amplitude area with few or no reflectors and appears homogenous. When compared to the area next to it, the multiple reflectors in this area appear stronger and are more observable. There is also a decrease in the slope gradient close to the dashed area, with the sediments on top following this slope, however the sediment and reflectors below show a more constant gradient across the graben. This profile also shows a high number of faults visible in the

glacial clay unit, which is characterized by multiple reflectors, as seen in figure 8A, which do not appear in figures 10 and 11. Towards the bottom-center of figure 12A, a large graben structure can be seen that is most likely the result of reverse faulting. In the sub-bottom profile in figure 12C, onlapping reflectors can be seen on the right side of image, with the sediments appearing more horizontal in the center of the graben. The reflectors appear to show synformal and antiformal structures but are smaller than those seen in figures 10D and E but are more abundant. The area near the surface (orange dashed line) of figure 12C also shows a homogenous zone where reflectors terminate, and appears to be located just above the glacial clay. Erosion has also taken place in this area as reflectors terminate at the lake floor boundary.

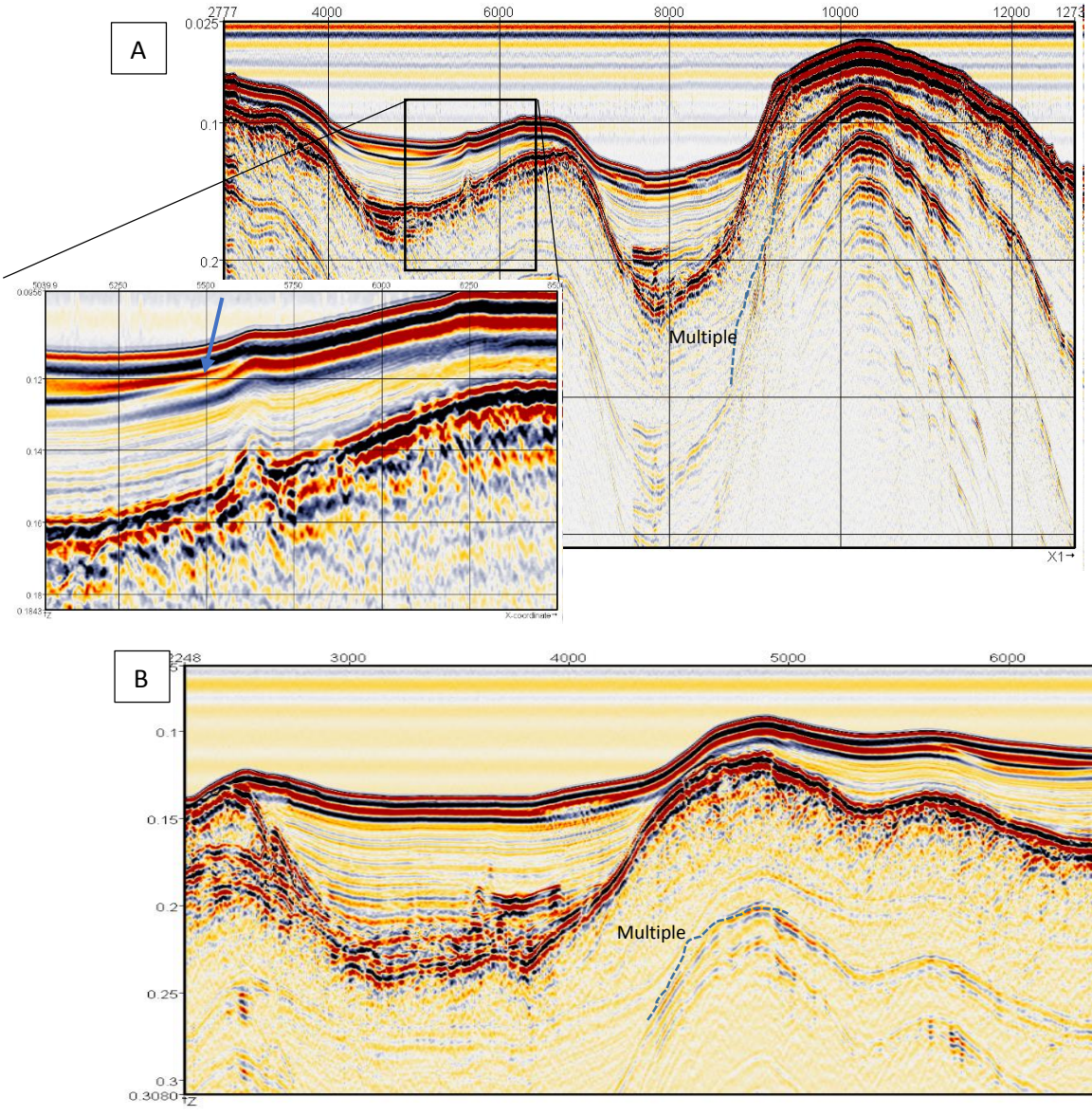

Figure 13: A: Seismic profile of line 220857. B: Seismic profile of line 165837. Both displaying undisturbed sediments.

In figure 13A, two depressions are evident in the bedrock, neither of which reach depths associated with the graben in figures 10 and 11. In the two depressions, the sediments have a TWTT of around 0.1 second in the deepest area, with the reflectors in a subhorizontal position with onlap occurring

in both depressions against the bedrock. Some deformation does occur in the profile, as in the first depression, sediment can be seen to flex upwards, and in the second depression, normal faulting appears in the upper-most gyttja clay sediment. Figure 13B is similar to 13A, with both profiles taken in close proximity, however the depression on the right of the profile appears to have a second, smaller 'U-shaped' depression present, along with the larger depression seen in the left side of the profile.

Multibeam Data

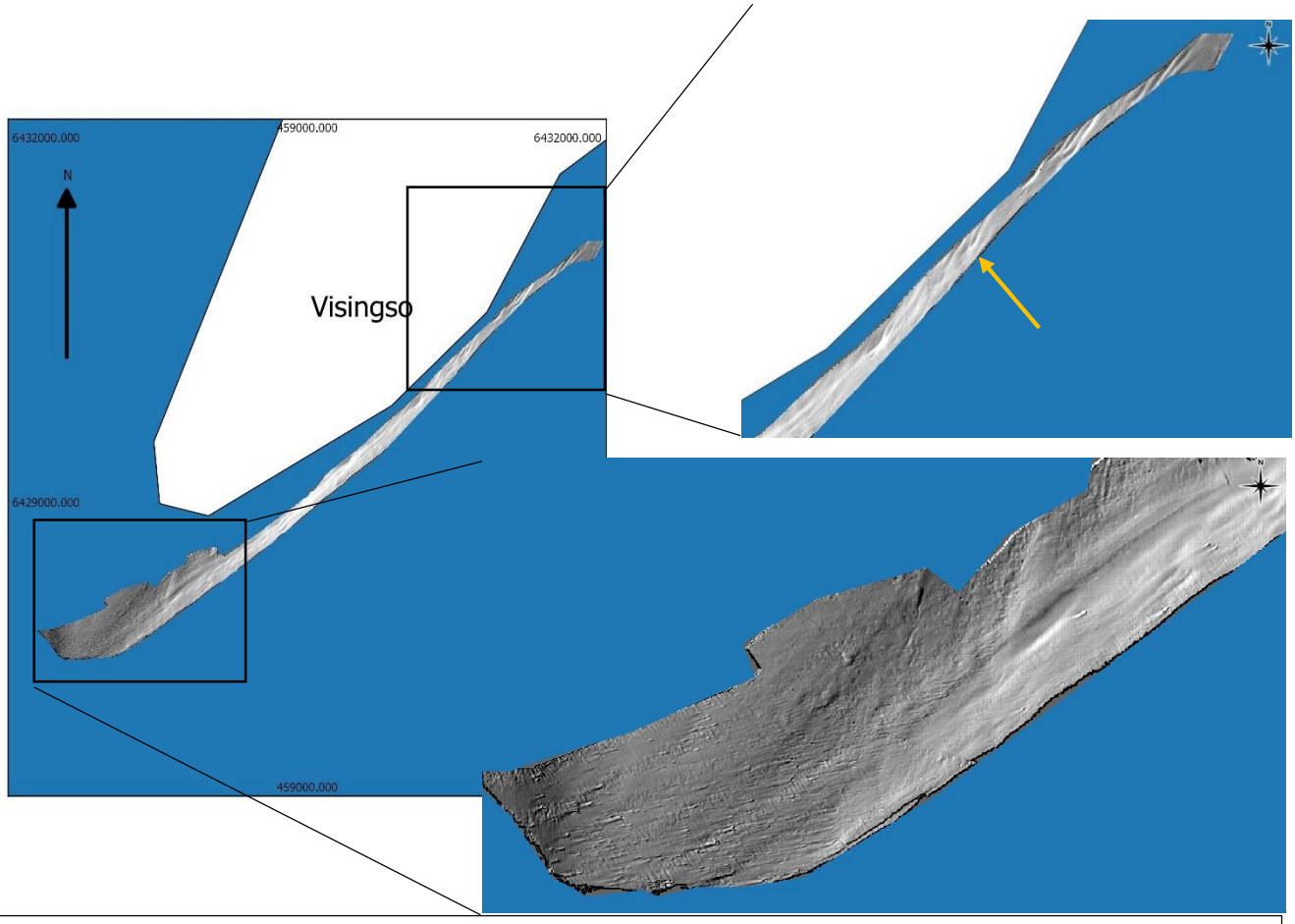

Figure 14: Multibeam data acquired along the east coast of Visingsö, displaying multiple surface morphological features.

Figure 14 displays the multibeam data acquired to the east and south of Visingsö as a hillshaded image with an azumuth of 135 and an angle from the horizontal of 10. From the image, small depressions are visible in the southern area that appear to have elongations to the south-east. There also appears to be some ridges that have formed that trend in a SE-NW direction, these are more apparent in the eastern area of Visingsö. In areas these form a staircase formation, whilst others appear to have a concaved geometery, which is similar to structures seen on the east side of the

strait (Jakobsson et al., 2014). In one of these areas, an offset can be seen between two bright areas (yellow arrow).

Figure 15 illustrates the distibution of the synform and antiform deformations that are evident in figures 10 and 11. From the figure, two large clusters are visible, one in the south of the Lake Vättern basin, and one east of Visingsö, with a number of synforms and antiforms present in the area between the two. These two clusters appear concentrated on the western side of the graben, which has a lower lake floor incline when compared with the western side.

Discussion

Bathymetric Map

The bathymetric map in figure 8 displays the graben structure seen in the lake that trends NE-SW in the area, with a steeper gradient located on the Eastern side, indicating an original asymmetrical graben formation. However, the detail provided from the bathymetric map generated by the seismic reflection data gives little insight into the lake floor and sediment structures that are present on the surface as they are a part of a 2D survey and do not provide the resolution required to analyze the surface in detail. Instead, multibeam mapping is required to analyze the surface in more detail.

Seismic Reflection and Sub-bottom

Seismic Stratigraphy

The information from table 2 and the correlation of core to reflectors in figure 8 allow the entire survey area to be resolved into the different sedimentary units to allow time constraints of deformation to be determined. Figures 9 – 13 display the interpreted units in the seismic profiles. The information presented by Swärd et al. (in review) gives a time constraint for each of the units, with the transition from glacial clay I to glacial clay II occurring around 14.6 ka, the boundary between glacial clay II and post-glacial clay occurring >11.5 ka, with the brackish water stage occurring between ~13.0 ka and 11.5 ka, based on porewater chlorine content (Swärd et al., in review).

Sediment Deformation

Gravitational Sliding

The location of the deformation of the uppermost sediment in both 9A and B indicates that both are due to gravitational slide processes of sediment down slope and not due to bedrock movement directly below, as neither of the faults in the figures reach the bedrock. However, this movement could be in response to bedrock movement in the deeper areas of the graben, which creates accommodation space for some of the sediment to move into. These faults in the sediment are similar to those presented by Upton and Osterberg (2007) and Bini et al. (2007).

Tectonic Activity

The synform and antiform structures visible in figure 10A and B are in response to faulting in the sediment below. These faults do not penetrate the surface, most probably due to the vertical resolution of the survey. They appear to show a range of structures, including grabens and stepped faults, displaying both normal and reverse senses. Faulting displayed in 10C is mainly a normal sense towards the depressions, but the main antiform in the profile appears to exist due to a pop-up structure. This indicates that the area underwent mainly compressive forces, similar to 10A and B. This also explains the long antiform but small synform structures seen. Some normal faulting is visible below the synform structures, whilst the surface expressions of these structures are up to 100 m wide and 10 m deep (Jakobsson et al., 2014), implying that the fault network generating these structures is a complicated, three-dimensional system. Due to the resolution of the seismic reflection data, it is unsure if the faulting occurs only in the sediments or if it extends into the bedrock below. Figures 10A and 10B also show the toplap of sediments, an indication of erosion and

subsequent depsostion, along with figures 10A, B and C displaying offlap of sediments onto the bedrock, which is evidence deposition on a slope. The sub-bottom profile in Figure 10D displays an area that has undergone little or no recent erosion, but not penetrating as far as the erosion seen from the toplap in figure 10A, whilst the sub-bottom profile in 10E displays an area that has undergone initial erosion and subsequent deposition.

The origin of these large depressions and elevations in figure 11 is most likely the same as in figure 10, with the reverse faulting in the area resulting in these large elevations and normal faulting resulting in depressions. From the sub-bottom image, the depression is slightly filled in, with the gyttja clay appearing undisturbed, but the area has undergone profuse erosion with glacial clay exposed on the lake floor. From the sub-bottom data an estimated displacement of 11 m is visible in the glacial clay unit. Some marginal toplap and onlap is seen in the seismic profile in figure 11A, but does not appear as pronounced as those seen in figure 10. When associated to figure 10, the synform is appears very large in comparison, most likely due to a larger normal fault. From the interpretation of units from the core shown in figure 8, the deformation appears to have occurred before the deposition of the gyttja clay. When analyzing the sub-bottom image in 11C, the majority of deformation is concentrated in the glacial clay, but the area appears to have undergone a large amount of erosion. The sub-bottom image also shows structures in the reflectors that appear to indicate ‘s’ and ‘z’ micro-folds.

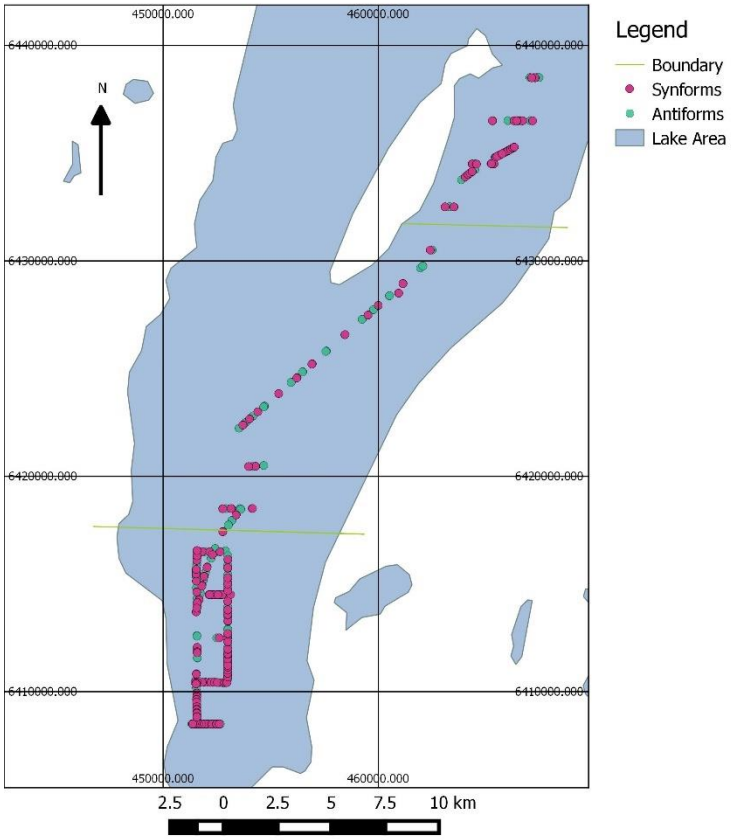

Figure 15: Zones of different deformation, along with the distribution of synformal and antiformal structures seen in the upper-most sediment.

Figure 12 presents a slump deposit that may have been caused by a paleoseismic event, due to being located within close proximity to the steep sides of the graben. Based on the seismic stratigraphy, the event occurred during the deposition of the glacial clay. This MTD is similar to those discussed in Lake Lucerne, Switzerland (Schnellmann et al. 2002), Canada (Shilts and Clague, 1992; Shilts et al.,

1992) and Lake Tekapo, New Zealand (Upton and Osterberg, 2007). Below this slump deposit, there appears to be a set of faulting that has occurred in the glacial clay that displays both normal but mainly reverse faulting across the profile. When analyzing the sub-bottom image of figure 12C, long antiform structures are visible with tight synform structures, similar to those seen in the reflection profiles in figure 10.

The difference in sediment deformation seen in between figures 10, 11 and 12 is characteristic for zones in the postion from the strike-slip fault. The highly faulted glacial clay that appears to show normal and reverse faulting figure 12 in focused in the center of the southern area of the lake, whereas the large fold structures seen in figure 10 and 11 are representative of the areas located in the south of the lake and east of Visingsö (figure 15). The sediment in figure 10 and 11 only display localized faulting below folds while in figure 11, the faults cause small folds in the sediment, but are only visible in the sub-bottom profile, indicating greater vertical displacement in figures 10 and 11. The core presented by Swärd et al. (in review) describes micro reverse faulting in the glacial clay, which can be associated with the southern area, representing reverse sense faults in the area.

The structures seen in figures 10 – 12 give rise to the idea of a neotectonic event causing deformation in the sediment that has been deposited in the region. Evidence of a positive flower structure in some of the seismic profiles provides evidence in support of a strike-slip fault in the region (Christie-Blick and Biddle, 1985). For further analysis, the deformation ellipse related to strike slip faulting is used (figure 16) using the location of the fold structures (figure 15). To satisfy the positioning of the folds and structures in figure 15, figure 16A and B has to be reversed to display left-lateral shear, indicating that the fault in the area underwent sisntral movement in the tectonic event that caused the sediment deformation. The position of the fault follows a similar trend to the graben axis and most likely occurred as a reactivation along this fault, which also corresponds to the central fault axis proposed by Jakobsson et al. (2014). These are dated at around the end of the younger dryas (11.5 ka yr. BP.) , however normal faults in the northern area of lake Vättern presented by Mörner (1985) give a date of 10 ka yr. BP based on the same boundary between late glacial and post glacial sediment deposition deposition. These fault systems most likely occurred along the same strike-slip, with areas of en echelon folds and formations in the south and extensional fracturing in the North.

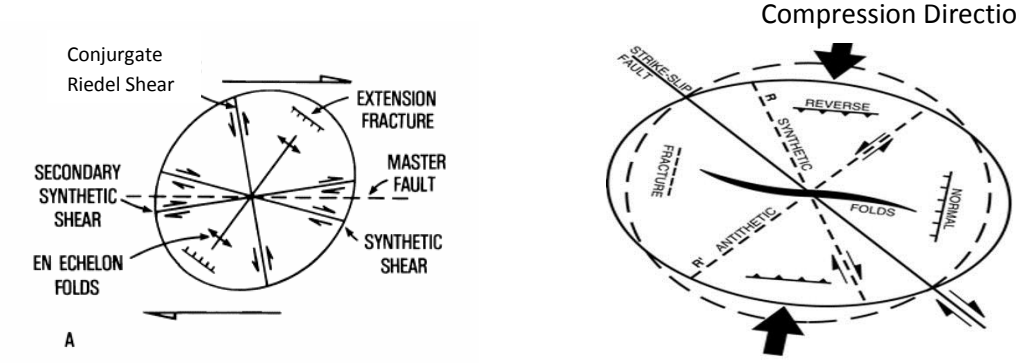

Figure 16: Deformation ellipse related to strike slip faulting displaying right-lateral simple shear A: Displaying perfect strike-slip conditions. (Modified from Christie-Blick and Biddle, 1985). B: Compressive forces resulting in strike slip movement (Modified from Law, Eriksson and Davisson, 2001).

The sub-bottom images allow a better understanding of what sediment has been deformed due to higher resolution, but only penetrates at most the top 10's of meters in the survey. From these, it can be determined that the deformed sediment is the glacial clay and sub-units, due to the multiple reflectors seen in the sub-bottom profiles. The deformation seen in the reflection profiles appear to effect the entire sediment column, indicating that the event took place around the end of the deposition of glacial clay, which has been dated to be around 11.5 ka cal. yr. BP by Swärd et al. (in review) from core analysis.

Glacial Processes

Figure 13 and the two depressions have a very different geometry to the graben and any other profiles that are display sediment in-filling. The geometry of both depressions appears to display an asymmetrical 'U-shape' that appears to have a steeper incline on the left side of both depressions. This, along with the shape of the elevated region between the two, implies a streamlined glacial erosion structure that formed due to subglacial erosion, similar to those portrayed in figure 17. The sediment deposited in the area appears mainly unaltered, with only minor normal faulting occurring in the larger depression in the uppermost sediment, and the draping of sediment over an extrusion of bedrock. The lack of deformation in these profiles displays that the deformation did not occur across the entire lake floor and implies that these areas were isolated from the deformation event.

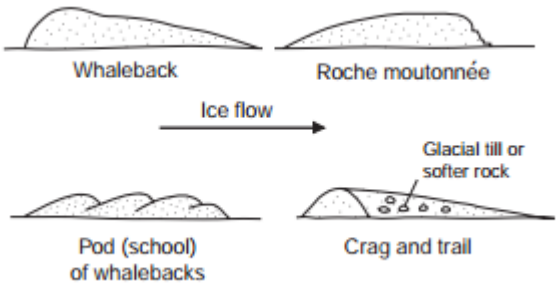

Figure 17: Four main types of streamlined glacial erosional landforms (Bennett and Glasser, 2009)

Multibeam

The elongations seen in figure 14 are most likely due to water expulstion from these depressions followed by bottom currents that cause erosion in the south-east direction. These ridges that appear in the image are most likely small rotational slumps resulting from fault movement in the sediment or bedrock below, creating slope instability and resulting in mass movement of sediment. The offset that is seen in figure 14 (arrowed) could possibly represent a strike-slip fault with apparent dextral movement.

Conclusion

The objective of this thesis was to better understand the complex quaternary history of the region through the analysis and interpretation of seismic data, along with information from complimentary sources, such as cores. The seismic data provide ample evidence of both glacial features and tectonic activity in the area, as well as cores providing some time constraints.

As discussed in the introduction, the seismic data exhibited in the observations and discussions sections agrees with the consensus that the lake was created through the formation of a graben (figures 9 – 12) as well as undergone subsequent glacial erosion during the last glacial maximum (figure 13). Visible faulting in the seismic profiles throughout the basin are concentrated in the glacial clay units and below. These fault tips do not visibly penetrate into the post-glacial clay above in any of the figures (9 – 13), though this may be due to the vertical resolution of the seismic reflection data. However, the sediment deformation appears to effect the sediment deposited within the graben, but not the sediment deposited in glacial erosional features.

The results can be summarised as follows:

- The bathymetry of the lake is still largely controlled by the shape of the graben, with the deep trough present following the NNW-SSE trend of the original graben structure.
- The depressions seen in figure 13 are clearly not in relation to the graben structure and are filled with horizontally deposited sediments that show no deformation patterns. This means the area was either: (1) formed after the tectonic event; or (2) isolated from its effects. Based on the seismic stratigraphy, the latter is favoured. Due to the sediment appearing to mainly consist of Quaternary deposits from the seismic analysis, it is evidence the formation originates from glacial erosion in the area.
- Sedimentation rates in the southern area appear to be low, along with active erosion, due to the appearance of glacial clay near the lake surface in the majority of sub-bottom profiles displayed in figures 9 – 12.
- The seismic profiles displaying synformal and antiformal structures within the sediment are concentrated to within the graben structure and the normal and reverse faults seen in the area are due to sinstral strike-slip faulting along a NNW-SSE trend and occurred as a result of compressional forces. Evidence is presented by positive flower structures observable in the seismic profiles, along with analysis from the deformation ellipse in figure 16. The faulting most likely occurred as a reactivation along faults in the region and could be in response to isostatic rebound from the unloading of the last Weichselian glaciation, drainage of the Baltic ice lake (Jakobbson et al., 2014), or basin inversion due to the general compressive stress field of the Baltic shield (Lund and Zoback, 1999). The faulting in the center region of the survey appears to be displayed in a stair case geometry, representing en echelon structures that tilt mainly in an easterly direction and display some extension. This is most likely due to the resultant forces from the stress field generated by the strike slip fault.

Further Research

To fully assess the quaternary history of Lake Vättern, a 3D seismic survey is required on the region to further understand the cause of the faulting in the glacial clay and the synformal and antiformal deformation of the sediment, as these structures are very unusual in a lacustrine environment.

Note on Software

The use of open source software has been a tiresome task, as OpendTect is mainly concentrated to 3D seismic surveys and requires prerequisite knowledge to make the most of the software. However, it has been very useful, if very slow at times, being able to work from anywhere as the program is free. Some things may have been presented differently throughout the paper, such as profiles in depth instead of two-way travel time and the use of migration. The software performs all basic tasks well, such as horizon and fault tracking, and is good for a beginner in seismic data interpretation to their improve knowledge on the software operations. Multiple 3D surveys are available for free to download from the opendtect website, along with guides and walkthroughs for practise that will be useful once in the workplace.

Acknowledgements

I would like firstly to thank Richard Gyllencreutz and Martin Jakobsson for providing the opportunity to work with the seismic data that they have collected from the Lake Vattern area and providing stellar assistance when required, as well as inspiring me in the marine geological mapping module. I would also like to thank my parents, friends and family who have supported me throughout university and my year abroad.

References

Andréasson, P. and Rodhe, A. (1990). Geology of the Protogine Zone south of Lake Vättern, southern Sweden: A reinterpretation. *Geologiska Foereningan i Stockholm. Foerhandlingar*, 112(2), pp.107-125.

Andrén, T., Lindeberg, G. and Andrén, E. (2002). Evidence of the final drainage of the Baltic Ice Lake and the brackish phase of the Yoldia Sea in glacial varves from the Baltic Sea. *Boreas*, 31(3), pp.226-238.

Axberg, S., and Wadstein, P. (1980). Distribution of the sedimentary bedrock in Lake Vättern, southern Sweden. *Acta Universitatis Stockholmiensis*, v. 34, p. 15–26.

Bennett, M. and Glasser, N. (2009). *Glacial geology*. Chichester, UK: Wiley-Blackwell, Pp. 150.

Bini, A., Corbari, D., Falletti, P., Fassina, M., Perotti, C. and Piccin, A. (2007). Morphology and geological setting of Iseo Lake (Lombardy) through multibeam bathymetry and high-resolution seismic profiles. *Swiss j geosci*, 100(1), pp.23-40.

Björck, S. (2008). The late Quaternary development of the Baltic Sea basin. In The BACC Author Team (Eds.): Assessment of climate change for the Baltic Sea Basin, *Springer-Verlag Berlin Heidelberg*, 398-407.

Brown, A.R. (2004). Interpretation of Three-Dimensional Seismic Data, sixth ed. AAPG Memoir, 42. *American Association of Petroleum Geologists*, Tulsa.

Christ, R. and Wernli, R. (2014). *The ROV manual*. 1st ed. Waltham, Mass.: Butterworth-Heinemann.

Clark, P., Dyke, A., Shakun, J., Carlson, A., Clark, J., Wohlfarth, B., Mitrovica, J., Hostetler, S. and McCabe, A. (2009). The Last Glacial Maximum. *Science*, 325(5941), pp.710-714.

Collini, B. (1951). Beskrivning till kartbladet Gränna. *Sveriges Geologiska Undersokning*, An 193, 1-100.

Collins English Dictionary. (2003). Collins English Dictionary – Complete and Unabridged. Retrieved April 10 2015 fromhttp://www.thefreedictionary.com/harmonic+mean

De Geer, S. (1910). Map of landforms in the surroundings of the great Swedish lakes. *SGU,* Ba 7.

Flodén, T. (1980). Seismic stratigraphy and bedrock geology of the Central Baltic. *Stockholm Contributions in Geol.,* 35, 1 - 240.

Forel, D., Benz, T. and Pennington, W. (2005). *Seismic data processing with Seismic Un*x*. Tulsa, Okla.: Society of Exploration Geophysicists. p. 3-1

Jakobsson, M., Björck, S., Alm, G., Andrén, T., Lindeberg, G. and Svensson, N. (2007). Reconstructing the Younger Dryas ice dammed lake in the Baltic Basin: Bathymetry, area and volume.Global and Planetary Change, 57(3-4), pp.355-370.

Kearey, P., Brooks, M. and Hill, I. (2002). An introduction to geophysical exploration. *Wiley-Blackwell*, 268 pp.

Lind, G. (1972). The Gravity and Geology of the Vättern area, Southern Sweden. *Geologiska Föreningens i Stockholm Förhandlingar*, 94:2, 245-257.

Lindh, G. (1972). The Gravity and Geology of the Lake Vättern Area, South Sweden. *GFF.* 94: 245-57.

Lund, B., and Zoback, M.D., (1999). Orientation and magnitude of in situ stress to 6.5 km depth in the Baltic Shield. *International Journal of Rock Mechanics and Mining Sciences*. v. 36, p. 169-190, doi: 10.1016/S0148-9062(98)00183-1.

Lundqvist, J. & Wohlfarth, B. (2001): Timing and east-west correlation of south Swedish ice marginal lines during the Late Weichselian. *Quaternary Science Reviews*, 20, 1127–1148

Lurton, X. (2010). An Introduction to Underwater Acoustics. Principles and Applications. Springer-Verlag: Berlin. ISBN: 978-3-540-78480-7

Månsson, A.G.M. (1996). Brittle reactivation of ductile basement structures; a tectonic model for the lake Vättern basin, southern Sweden. *GFF*, 118(sup004), pp.19-19.

Milnes A.G., Gee D.G., Lund K-E. (1998). Crustal structure and regional tectonics of SE Sweden and the Baltic Sea. *SKB T-R-98-21, Swedish Nuclear Fuel and Waste Management* Co. 58 p.

Navipedia (2015). *SBAS Fundamentals - Navipedia*. [online] Available at: http://www.navipedia.net/index.php/SBAS_Fundamentals [Accessed 4 Mar. 2015].

OGP Report (2011). An overview of marine seismic operations. *IAGC.* Report No. 448.

Park, R. (2013). *Foundation of Structural Geology*. Hoboken: Taylor and Francis. Pp. 22

Parkes, G. and Hatton, L. (1986). *The marine seismic source*. Dordrecht: D. Reidel.

Randall, R.E., (2008). Elements of Ocean Engineering. 2nd edition. *Society of Naval Architects and Marine Engineers (SNAME)*. ISBN: 978-0-939773-77-0.

Sandersen, P. and Jørgensen, F. (2014). Neotectonic deformation of a Late Weichselian outwash plain by deglaciation-induced fault reactivation of a deep-seated graben structure. *Boreas*, 44(2), pp.413-431.

Schnellmann M., Anselmetti F.S., Giardini D., McKenzie J.A., Ward S.N. (2002). Prehistoric earthquake history revealed by lacustrine slump deposits. *G*eology 30: 1131–1134

SGU (Geological Survey of Sweden), (2010). Bedrock Sweden 1:1 000 000. Electronic Resource: https://maps.slu.se/get

Shilts W., Rappol W.M., Blais A. (1992). Evidence of late and postglacial seismic activity in the Témiscouata–Madawaska Valley, Quebec–New Brunswick, Canada. *Canadian Journal of Earth Sciences* 29: 1043–1069.

Shilts W.W., Clague J.J. (1992). Documentation of earthquake-induced disturbance of lake sediments using subbottom acoustic profiling. *Canadian Journal of Earth Sciences* 29: 1018–1042.

Söderlund, P., Söderlund, U., Möller, C., Gorbatschev, R. and Rodhe, A. (2004). Petrology and ion microprobe U-Pb chronology applied to a metabasic intrusion in southern Sweden: A study on zircon formation during metamorphism and deformation. *Tectonics*, 23(5), p.1-16

Söderlund, U., Isachsen, C., Bylund, G., Heaman, L., Jonathan Patchett, P., Vervoort, J. and Andersson, U. (2005). U–Pb baddeleyite ages and Hf, Nd isotope chemistry constraining repeated mafic magmatism in the Fennoscandian Shield from 1.6 to 0.9 Ga. *Contributions to Mineralogy and Petrology*, 150(2), pp.174-194.

Sonographics (2014). Sonographics, Inc. - EdgeTech SB-216S Sub-bottom Profiler. [online] Available at: http://www.sonographics.net/216.htm [Accessed 4 Mar. 2015].

Steele, J., Thorpe, S. and Turekian, K. (2001). *Encyclopedia of ocean sciences*. San Diego: Academic Press. P. 579-588

Svendsen, J. I., et al. (2004), Late Quaternary ice sheet history of northern Eurasia, Quaternary Science Reviews, 23(11-13), 1229-1271, doi:10.1016/j.quascirev.2003.12.008.

Swärd, H., O´Regan, M., Ampel, L., Ananyev, R., Chernykh, D., Flodén, T., Greenwood, S.L., Kylander, M., Mörth, C-M., Preto, P., and Jakobsson, M. (in press). Regional deglaciation and postglacial lake development as reflected in a 74 m sedimentary record from Lake Vättern, southern Sweden, GFF.

Trabant, P. (1984). *Applied high-resolution geophysical methods*. Boston: International Human Resources Development Corp.

Vidal, G. (1974). Late Precambrian Microfossils from the Basal Unit of the Visingsö Beds in South Sweden. *Geologica et Paläontographica*, 8 (Marburg).

Law, R., Eriksson, K. and Davisson, C. (2001). Formation, evolution, and inversion of the middle Tertiary Diligencia basin, Orocopia Mountains, southern California. *Geological Society of America Bulletin*, 113(2), pp.196-221.